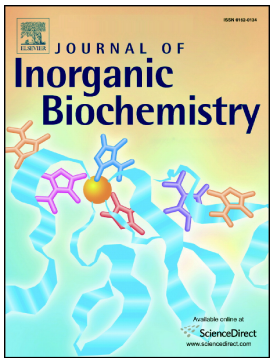

The N-terminal domain of Helicobacter Pylori's Hpn protein: The role of multiple histidine residues

Denise Bellotti, Angelica Sinigaglia, Remo Guerrini, Erika Marzola, Magdalena Rowińska-Żyrek, Maurizio Remelli

PII: S0162-0134(20)30332-9

DOI: https://doi.org/10.1016/j.jinorgbio.2020.111304

Reference: JIB 111304

To appear in: *Journal of Inorganic Biochemistry*

Received date: 30 July 2020

Revised date: 27 October 2020

Accepted date: 27 October 2020

Please cite this article as: D. Bellotti, A. Sinigaglia, R. Guerrini, et al., The N-terminal domain of Helicobacter Pylori's Hpn protein: The role of multiple histidine residues, *Journal of Inorganic Biochemistry* (2018), https://doi.org/10.1016/j.jinorgbio.2020.111304

The N-terminal domain of *Helicobacter Pylori*'s Hpn protein: the role of multiple histidine residues

Denise Bellotti,[a,b] Angelica Sinigaglia,[a] Remo Guerrini,[a] Erika Marzola,[a] Magdalena Rowińska-Żyrek,[b] Maurizio Remelli*[a]

[a] *Department of Chemical and Pharmaceutical Sciences, University of Ferrara, Via L. Borsari 46, 44121, Ferrara, Italy. E-mail: rmm@unife.it*

[b] *Faculty of Chemistry, University of Wrocław, F. Joliot-Curie 14, 50-383, Wrocław, Poland.*

Denise Bellotti, OrcID: 0000-0002-2634-0228

Maurizio Remelli, OrcID: 0000-0002-5705-3352

Remo Guerrini, OrcID: 0000-0002-7619-0918

Erika Marzola, OrcID: 0000-0002-1428-1363

Magdalena Rowińska-Żyrek, OrcID: 0000-0002-0425-1128

Abstract

Helicobacter pylori is a gram-negative bacterium with gastric localization that can cause many gastrointestinal disorders. Its survival in the host environment strictly requires an efficient regulation of its metal homeostasis, in particular of Ni(II) ions, crucial for the synthesis of some essential enzymes. Hpn is a protein of 60 amino acids, 47% of which are histidines, expressed by *H. pylori* and avid for nickel, characterized by the presence of an ATCUN (Amino Terminal Cu(II)- and Ni(II)-binding) motif and by two further histidine residues which can act as additional metal anchoring sites. We decided to deepen the following aspects: *(i)* understanding the role of each histidine in the coordination of metal ions; *(ii)* comparing the binding affinities for Cu(II), Ni(II) and Zn(II) ions, which are potentially competing metals *in vivo*; *(iii)* understanding the Hpn ability of forming ternary and poly-nuclear complexes. For these purposes, we synthesised the Hpn N-terminal "wild-type" sequence (MAHHEEQHG-Am) and the following peptide analogues: MAAHEEQHG-Am, MAHAEEQHG-Am, MAHHEEQAG-Am and MAHAEEQAG-Am. Our results highlight that the histidines in position 4 and 8 lead to the formation of Cu(II) binuclear complexes. The ATCUN motif is by far the most efficient binding site for Cu(II) and Ni(II), while macrochelate Zn(II) complexes are formed thanks to the presence of several suitable anchoring sites (His and

Glu). The metal binding affinities follow the order Zn(II) < Ni(II) << Cu(II). In solutions containing equimolar amount of wild-type ligand, Cu(II) and Ni(II), the major species above pH 5.5 are hetero-binuclear complexes.

Keywords

Copper, Nickel, Zinc, Metal complexes, Hpn protein, ATCUN motif

Introduction

Helicobacter pylori is a spiral-shaped gram-negative bacterium that can survive and proliferate in the human stomach; it is present in about half of the Earth population. *H. pylori* infection can cause serious disorders such as gastro-duodenal ulcer, MALT (mucosa-associated lymphoid tissue) lymphoma and gastric cancer, which is responsible for almost one million deaths worldwide every year [1]. The World Health Organization has classified *H. pylori* as a "Group 1" human carcinogen [2]. The survival capacity of the bacterium is especially based on the activity of urease, a nickel-containing enzyme that catalyzes the hydrolysis of urea to ammonia and bicarbonate which act as buffers and allow *H. pylori* to keep neutral the pH of its cytoplasm [3]. Urease represents about 10% of the total soluble proteins of *H. pylori* and requires up to 24 nickel ions [4]. Another enzyme that contains nickel, and also important for *H. pylori*, is the [NiFe] hydrogenase, which allows the bacterium to exploit molecular hydrogen as an alternative energy source [5].

Nickel is therefore crucial for the virulence of *H. pylori*, which contains a rather complicated management system for the homeostasis of this metal ion. This system includes a small cytoplasmic protein, called Hpn (*Helicobacter pylori* protein with affinity for nickel) [6], rich in histidine, which accounts for about 2% of the total synthesized proteins.

The role played by Hpn in *H. pylori* is not fully understood; this protein was initially considered to store nickel in the cell and to alleviate the metal toxicity by sequestering the intracellular excess of nickel [7]. In fact, it was reported that *H. pylori* mutants with Hpn deficiencies are more sensitive to excess of Ni(II) than the wild-type bacterium [8]. Interestingly, it has also been observed that, under acidic conditions, Hpn releases the bound nickel and it has been suggested that this allows the protein to supply nickel to the cell when urease activity needs to be stimulated for pH regulation [9, 10]. Recently, it has also been proposed that Hpn interacts

with many other proteins to perform various cellular functions connected with the maturation of enzymes that contain nickel, with the recovery of peptides and the acquisition of nitrogen [2].

Using equilibrium dialysis and subsequent analysis by ICP-MS and UV/visible spectrophotometry, Ge et al. have shown that Hpn binds five Ni(II) ions per monomer at pH 7.4 [11]; however, the measured dissociation constant was quite modest (K_d = 7.1·10^{-6} mol dm^{-3}). A more recent study has confirmed that Hpn can bind up to six Ni(II) ions per monomer [12]. On the other hand, an investigation carried out by converting Hpn into a FRET-based fluorescent sensor [13] reported a K_d value *in vitro* as low as 7.89·10^{-8} mol dm^{-3}, while it was not possible to measure any affinity of the Hpn-FRET (Förster resonance energy transfer) probe for Ni(II) within *E. coli*, most likely due to the severe control of the levels of this potentially toxic metal inside the cell.

MAHHEEQHG^{10} HHHHHHHTHH^{20} HHYHGGEHHH^{30} HHHSSHHEEG^{40} CCSTSDSHHQ^{50} EEGCCHGHHE^{60}

Scheme 1. Amino acid sequence of Hpn protein. The studied N-terminal fragment is underlined; His residues are shown in green and Cys residues in red.

Hpn contains 60 amino acids, 28 of which (47%) are histidines [6]) (see Scheme 1). Hpn has several domains capable of coordinating metal cations [14-16], such as the poly-histidine sequences in the positions 11–17, 18-26 and 28–33 [14], the two motifs encompassing a double cysteine residue (EEGCC), in the positions 38–42 and 51–55 [17] and the amino-terminal sequence (Met-Ala-His-), containing a His residue in the third position, which makes it particularly suitable to bind divalent metal ions such as Cu(II) and Ni(II) [18, 19]. The coordination ability of this latter sequence, called "ATCUN" (Amino Terminal Cu(II)- and Ni(II)-binding motif) is highly recognized [20] and it has already been studied in the past by our research team, but only in conditions of ligand excess [18].

Although the first three Hpn residues play a major role in the Hpn binding ability towards Ni(II), the additional histidines in positions 4 and 8 can have a non-negligible effect on the stability of the metal complexes, for two main reasons: (i) they can take part in the formation of complexes, forming macrochelated species; (ii) they can anchor a second metal ion. We therefore decided to take a deeper look to these aspects by following two main lines of investigation. First, comparing the affinity towards the Cu(II), Ni(II) and Zn(II) ions of the model peptide corresponding to the N-terminal domain of Hpn, MAHHEEQHG-Am (wild-type, **WT**), with that of its mutants

obtained by substitution of one or two His residues with alanine (Ala-scan): MAAHEEQHG-Am (**H3A**), MAHAEEQHG-Am (**H4A**), MAHHEEQAG-Am (**H8A**) and MAHAEEQAG-Am (**H4A/H8A**) (Scheme S1, SI†). All the peptides are protected by amidation at their C-terminus to better simulate the behaviour of the entire protein. Second, in the case of the cupric ion, the complex-formation equilibria under condition of metal excess have been studied, in order to detect the formation of binuclear complexes. Stoichiometry and thermodynamic stability of the formed species have been studied by mass spectrometry and potentiometry under a wide range of pH; the structural hypotheses of the main complexes detected in solution have been suggested on the basis of the results of several spectroscopic techniques.

Experimental

Materials

$CuCl_2$, $ZnCl_2$ and $NiCl_2$ were extra pure products (Sigma-Aldrich); the concentrations of their stock solutions were standardised by EDTA titration and periodically checked *via* ICP-OES. The carbonate-free stock solutions of 0.1 mol dm^{-3} KOH were prepared by diluting concentrated KOH (Sigma-Aldrich) and then potentiometrically standardized with the primary standard potassium hydrogen phthalate (99.9% purity). All sample solutions were prepared with freshly prepared Milli-Q® water. The HCl and HNO_3 stock solutions were prepared by diluting concentrated ultra-pure HCl and HNO_3 (Sigma-Aldrich) and then standardized with KOH. The ionic strength was adjusted to 0.1 mol dm^{-3} by adding KCl (Sigma-Aldrich). Grade A glassware was employed throughout.

Peptide synthesis and purification

All the peptides were synthesized according to published methods [21] using Fmoc (fluorenylmethoxycarbonyl protecting group)/t-butyl chemistry with a Syro XP multiple peptide synthesizer (MultiSynTech GmbH, Witten Germany). Rink amide MBHA resin was used as a solid support for the synthesis of all derivatives. Fmoc-amino acids (4-fold excess) were sequentially coupled to the growing peptide chain using DIPCDI/HOBt (N,N'-diisopropylcarbodiimide/1-hydroxybenzotriazole) (4-fold excess) as activating mixture for 1h at room temperature. Cycles of deprotection of Fmoc (40% piperidine/ N,N-dimethylformamide) and coupling with the subsequent amino acids were repeated until the desired peptide-bound resin was completed. N-

terminal acetylation has been performed with acetic anhydride (0.5 mol dm^{-3}) with the presence of N-methylmorpholine (0.25 mol dm^{-3}) (3:1 v/v; 2 mL / 0.2 g of resin) as the last synthetic step. The protected peptide-resin was treated with reagent B [22] (trifluoroacetic acid (TFA) / H20 / phenol / triisopropylsilane 88 : 5 : 5: 2; v/v; 10 mL / 0.2 g of resin) for 1.5 h at room temperature. After filtration of the resin, the solvent was concentrated in vacuo and the residue triturated with ethyl ether. Crude peptides were purified by preparative reversed-phase HPLC using a Water Delta Prep 3000 system with a Jupiter column C18 (250 x 30 mm, 300 A, 15 µm spherical particle size). The column was perfused at a flow rate of 20 mL/min with a mobile phase containing solvent A (5%, v/v, acetonitrile in 0.1% TFA), and a linear gradient from 0 to 30% of solvent B (60%, v/v, acetonitrile in 0.1% TFA) over 25 min for the elution of peptides. Analytical HPLC analyses were performed on a Beckman 116 liquid chromatograph equipped with a Beckman 166 diode array detector. Analytical purity of the peptides has been assessed using a Zorbax C18 column (4.6 x 150 mm, 3 µm particle size) with the above solvent system (solvents A and B) programmed at a flow rate of 0.5 mL / min using a linear gradient from 0% to 50% B over 25 min. All analogues showed ≥ 95% purity when monitored at 220 nm. Molecular weight of final compounds was determined by a mass spectrometer ESI Micromass ZMD-2000.

Potentiometry

Stability constants for proton and metal complexes were calculated from pH-metric titration curves registered at *T*=298 K and ionic strength 0.1 mol dm^{-3} (KCl). The potentiometric apparatus consisted of an Orion EA 940 pH-meter system provided with a Metrohm 6.0234.100, glass-body, micro combination pH electrode and a dosing system Hamilton MICROLAB 500, equipped with a 0.5 ml micro burette. The thermostated glass-cell was equipped with a magnetic stirring system, a microburet delivery tube and an inlet-outlet tube for the inert gas. High purity grade nitrogen was gently blown over the test solution in order to maintain an inert atmosphere. A constant-speed magnetic stirring was applied throughout. Solutions were titrated with 0.1 mol dm^{-3} carbonate-free KOH. The electrode was daily calibrated for hydrogen ion concentration by titrating HNO_3 with alkaline solution under the same experimental conditions as above. The standard potential and the slope of the electrode couple were computed by means of SUPERQUAD [23] and Glee [24] programs. The purities and the exact concentrations of the ligand solutions were determined by the Gran method [25]. The HYPERQUAD [26] program was employed for the overall formation constant (β) calculations, referred to the following equilibrium:

$$pM + qL + rH \leftrightarrows M_pL_qH_r$$

(charges omitted; *p* is 0 in the case of ligand protonation; *r* can be negative). Step formation constants (K_{step}) and/or acid dissociation constants (K_a) are also reported. The computed standard deviations (referring to random errors only) were given by the program itself and are shown in parentheses as uncertainties on the last significant figure. Hydrolysis constants for metal ions were taken from the literature and suitably extrapolated for the experimental conditions here employed [27, 28]. The distribution and the competition diagrams were computed using the HYSS program [29]. In particular, the latter are calculated from the binary speciation models, hypothesizing a solution containing the metal and the various ligands, and admitting that all the components compete with each other to form the respective binary complexes, without mixed species formation.

Mass spectrometry

High-resolution mass spectra were obtained on a BrukerQ-FTMS spectrometer (Bruker Daltonik, Bremen, Germany), equipped with an Apollo I electrospray ionization source with an ion funnel and on a linear ion trap LTQ XL Mass Spectrometer (Thermo Scientific, Waltham, MA, USA). The mass spectrometer was operated in the positive ion mode. The instrumental parameters for BrukerQ-FTMS spectrometer were as follows: scan range m/z 100–2500, dry gas nitrogen, temperature 453 K and ion energy 5 eV. The capillary voltage was optimized to the highest signal-to-noise ratio, corresponding to 4200 V. Experimental conditions for LTQ XL Mass Spectrometer were as follows: spray voltage 4.8 kV; sheath gas 40 a.u.; capillary temperature 523 K; capillary voltage 8–25 V and tube lens 60–120 V. The samples were prepared in a 1:1 methanol-water mixture at different pH values. The samples ($[ligand]_{tot}=5\cdot10^{-4}$ mol dm^{-3}) were directly infused at a flow rate of 3 µL min^{-1}. Data were processed using the Bruker Compass DataAnalysis 3.4 program. The mass accuracy for the calibration was better than 5 ppm, enabling together with the true isotopic pattern (using SigmaFit) an unambiguous confirmation of the elemental composition of the obtained complex.

Spectroscopic measurements

The absorption spectra were recorded on a Varian Cary50 Probe spectrophotometer, in the range 350–900 nm, using a quartz cuvette with an optical path of 1 cm. Circular dichroism (CD) spectra were recorded on a Jasco J-1500 CD spectrometer in the 200–800 nm range, using a quartz cuvette with an optical path of 1 cm in the visible and near-UV range. Electron paramagnetic resonance (EPR) spectra were recorded in liquid nitrogen on a Bruker ELEXSYS E500 CW-EPR spectrometer at X-band frequency (9.5 GHz) and equipped with an ER 036TM NMR teslameter and an E41 FC frequency counter. Ethylene glycol (30%) was used as a cryoprotectant for EPR measurements. The EPR parameters were analysed by computer simulation of the experimental spectra using WIN-EPR SIMFONIA software, version 1.2 (Bruker). The concentrations of sample solutions used for spectroscopic studies were similar to those employed in the potentiometric experiment. The UV-Vis, CD and EPR spectroscopic parameters were calculated from the spectra obtained at the pH values corresponding to the maximum concentration of each particular species, based on distribution diagrams.

Results and Discussion

Ligand protonation

The five investigated peptides possess two neighbouring Glu residues containing a carboxylic side chain which can release a proton, therefore, they can be represented as H_2L. In addition to these acidic residues, the peptides contain up to three histidines and the unprotected N-terminal amine, which is the most basic group in these ligands. The protonation constants are reported in Table 1, together with the available literature values; representative distribution diagrams are shown as Supplementary Information (Figs. S1-S5).

Table 1. Overall (log *β*) and step (log *K*) protonation constants for the studied peptides at *T*=298 K and *I*=0.1 mol dm^{-3} (KCl). WT - MAHHEEQHG-Am; H3A - MAAHEEQHG-Am; H4A - MAHAEEQHG-Am; H8A - MAHHEEQAG-Am; H4A/H8A - MAHAEEQAG-Am. Values in parentheses are standard deviations on the last significant figure.

	WT				**H3A**		**H4A**		**H8A**		**H4A/H8A**	
Species	**log*β***	**log*K***	**log*β*** [a]	**log*K*** [a]	**log*β***	**log*K***	**log*β***	**log*K***	**log*β***	**log*K***	**log*β***	**log*K***
HL^-	7.79(2)	7.79	7.76	7.76	7.81(2)	7.81	7.70(3)	7.70	7.59(1)	7.59	7.59(1)	7.59
H_2L	14.75(1)	6.96	14.69	6.93	14.58(2)	6.77	14.58(3)	6.88	14.41(1)	6.82	14.16(1)	6.57

H_3L^+	21.34(2)	6.59	21.22	6.53	20.87(3)	6.29	20.80(4)	6.22	20.39(2)	5.98	18.76(2)	4.60
H_4L^{2+}	27.06(1)	5.72	27.02	5.80	25.37(2)	4.50	25.24(5)	4.44	24.70(2)	4.31	22.43(2)	3.67
H_5L^{3+}	31.20(2)	4.14	31.17	4.15	28.89(4)	3.52	28.64(3)	3.40	28.29(2)	3.59	-	-
H_6L^{4+}	34.59(2)	3.39	34.56	3.39	-	-	-	-	-	-	-	-

[a] Witkowska et al. [18]

The protonation constants measured in the present work for the wild-type peptide are almost identical to the values previously reported [18]; in the case of mutants, no literature value is available but the present results are in excellent agreement with literature data of other peptides containing the same residues with acid/base properties [30]. The substitution of one or two His residue with Ala does not affect the basicity of the terminal amine, whose log*K* value ranges in a very narrow interval (7.59 – 7.81). As for the Glu residues, the most acidic of them is characterized by a log*K* value of 3.39 – 3.59 while the second one by a log*K* value of 4.14 – 4.60; their acidity increases (and the protonation constant decreases) with the charge of the ligand which in turn depends on the number of (protonated) His residues. Finally, the log*K* value of the side imidazole groups of histidines spans in the range 5.72 – 6.96; the available data do not allow to exactly attribute a protonation value to the single His residues, in terms of *micro*-constants. The Ala-scan is unable to identify significant differences in the acidity/basicity of the three single histidines and the only observable trend is the same already reported above for Glu residues: the higher the charge of the peptide, the lower the side-imidazole protonation-constant.

Binary Cu(II) complexes

*MAHHEEQHG-Am (wild-type **WT**)*

As observed above, the N-terminal fragment of Hpn investigated here contains an ATCUN-type metal-binding site, corresponding to the first three residues MAH-, the presence of which strongly characterize the Cu(II) and Ni(II) binding behaviour of this peptide. In a previous investigation on this system [18], performed in the presence of an excess of ligand, only the ATCUN-type coordination mode ($N_{Imidazole}$, N_{NH2}, $2N_{amide}$) was detected and the formation of only mononuclear 1:1 complexes was reported. In that case, only His in position 3 was claimed to be involved in complexation. However, the presence of two additional His residues can lead to the formation of binuclear complexes also in solutions containing Cu(II) and **WT** in equimolar amount. Therefore,

we decided to revisit this system and to extend the investigation to the case of excess of metal ion and to four new mutants where one or two histidines have been replaced by alanine.

As reported in the Experimental section, the thermodynamic investigation of complex-formation equilibria has been performed by means of potentiometric titrations on solutions where the M:L stoichiometric ratio was 0.8:1 or 1.9:1. The speciation model for the system Cu(II)/**WT**, reported in Table 2, was obtained putting all the experimental data together (8 curves, 753 experimental points in the pH range 2.5-11) and a very good fitting was obtained (σ = 1.81). Of course, given the speciation model, the shape of the corresponding distribution diagram depends on the metal and ligand concentrations: Fig. 1a shows that, when Cu(II) and **WT** are present in solution at a nearly equimolar ratio, six variously protonated mononuclear 1:1 complexes are formed in the explored pH range and they engage all the copper at pH higher than 5.2. The corresponding stoichiometries and formation constants are in very good agreement with literature values. However, at acidic pH, when "free" Cu(II) ions are still available in solution, a not negligible amount of the binuclear species $[Cu_2H_{-1}L]^+$ is formed (about 12%). On the other hand, if the metal ion is in excess, practically only binuclear complexes are formed at neutral/alkaline pH (Fig. 1b).

Table 2. Cumulative complex-formation constants (β) and acid dissociation constants (K_a) of Cu(II) complexes with the peptide MAHHEEQHG-Am (**WT**), at T = 298.2 K and I = 0.1 mol dm^{-3} (KCl). Standard deviations on the last figure in parentheses.

Species	**log β**	**pK_a**	**log β** [a]	**pK_a** [a]
$[CuH_3L]^{3+}$	25.52(8)	4.03	-	-
$[CuH_2L]^{2+}$	21.49(6)	4.39	-	-
$[CuHL]^{+}$	17.10(3)	4.57	17.38	4.72
[CuL]	12.53(2)	6.17	12.66	5.96
$[CuH_{-1}L]^{-}$	6.36(3)	7.05	-6.70	7.09
$[CuH_{-2}L]^{2-}$	-0.69(4)	-	-0.39	-
$[Cu_2H_{-1}L]^{+}$	10.98(2)	5.52	-	-
$[Cu_2H_{-2}L]$	5.46(3)	-	-	-
$[Cu_2H_{-4}L]^{-2}$	-9.27(3)	9.04		-
$[Cu_2H_{-5}L]^{-3}$	-18.31(5)	-	-	-

[a] Witkowska et al. [18]

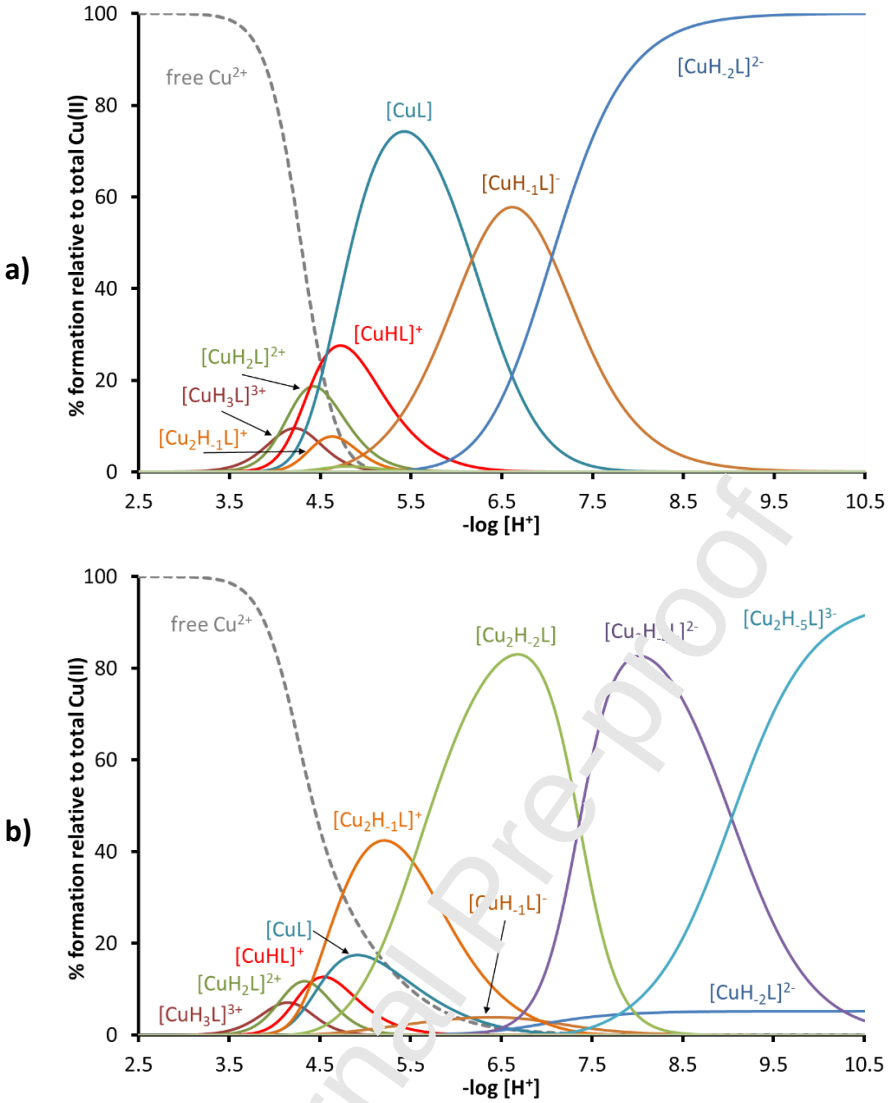

Fig. 1. Representative species distribution diagrams for complex-formation of **WT** with Cu(II), at T = 25 °C and I = 0.1 mol dm^{-3} (KCl). C_L = 1.0·10^{-3} mol dm^{-3} and a) $C_{Cu(II)}$ = 0.8·10^{-3} mol dm^{-3}; b) $C_{Cu(II)}$ = 1.9·10^{-3} mol dm^{-3}.

Starting from pH 3.5, the first detected species is $[CuH_3L]^{3+}$, whose stoichiometry indicates that only three residues involved in acid-base reactions are protonated: it is reasonable to assume that the two glutamic acids and a histidine residue are deprotonated. However, at such a pH value, histidine can be deprotonated only if it is coordinated to Cu(II) through the imidazole nitrogen of its side chain (N_{Im}); the participation of one or both carboxylate groups in chelation cannot be excluded. The species $[CuH_3L]^{3+}$ deprotonates with pK_a = 4.03 (see Table 2 and mass spectrum in Fig. S6, SI†); this value can be explained with the coordination of the terminal amine to form the species $[CuH_2L]^{2+}$, characterized by a "macrocyclic" coordination mode (N_{Im}, NH_2) [31]. By increasing the pH value, the species $[CuHL]^+$ and [CuL] begin to form, almost simultaneously, with

pK_a values of 4.39 and 4.57, respectively, compatible with the deprotonation and coordination of two amide nitrogens of the peptide chain, which occupy two further equatorial positions in the coordination sphere of the metal ion. This is the "ATCUN coordination mode": (N_{Im}, NH_2, $2N^-$). In excess of ligand (Fig. 1a), the species [CuL] reaches its formation maximum at pH 5.5 and dominates in solution in the range of pH 4.7 – 6.1, approximately. Since the formation of the first protonated species is extremely overlapped in a narrow pH range, the possibility of formation of binding isomers cannot be excluded. It is worth of note that, also in the presence of a slight excess of peptide with respect to Cu(II) (see the distribution diagram of Fig. 1a), in the acidic pH range, a not negligible amount of the binuclear $[Cu_2H_{-1}L]^+$ species is formed. Its possible structure is discussed below where the results of the investigation in excess of metal are reported.

From the qualitative Vis absorption spectra (Fig. S7, SI†) recorded at pH lower than 5.0, it is not possible to precisely identify the wavelengths of maximum absorption corresponding to the species $[CuH_3L]^{3+}$ $[CuH_2L]^{2+}$ and $[CuHL]^+$, due to the superimposition of these complexes and the interference of the exa-aquo Cu(II) ion, present in solution in a consistent amount up to pH 4.5. In the case of nearly equimolar Cu(II)/**WT** solutions, the UV-Vis spectra recorded at pH 5.0 and 5.5 are instead characterized by a single intense absorption band located at 525 nm (Fig. S7a and Table S1, SI†), almost entirely attributable to [CuL] and compatible with the coordination hypothesis (N_{Im}, NH_2, $2N^-$) suggested above (expected λ_{max} = 531 nm [32]). EPR data at pH 5.5 (Table S1, SI†) agree with a 4N coordination around Cu(II) in the equatorial plane of the complex [33]. Above pH 4.5, CD spectra (Fig. S8a and Table S1, SI†) contain two intense negative bands and one positive signal in the UV region, at 236, 272 and 311 nm, attributable to charge-transfer transitions to Cu(II) by the coordinated amine, imidazole and peptide nitrogens, respectively [34]. As for the Vis range of CD spectra, the typical double band characteristic of the ATCUN-type coordination [20] was observed. No clue was detected of a possible direct involvement of methionine sulphur in peptide coordination.

Finally, again in the presence of ligand excess (Fig. 1a), at neutral/alkaline pH, the species $[CuH_{-1}L]^-$ and $[CuH_{-2}L]^{2-}$ are formed, through two deprotonation steps involving the remaining two histidine residues, which do not participate in the complex formation. In fact, the corresponding pK_a values are respectively 6.17 and 7.05 (Table 2), rather close to those obtained for the free ligand (6.59 and 6.96) (Table 1). This hypothesis is also confirmed by all the spectroscopic data which do not change by increasing the pH value from 5 to 10, as expected if the coordination mode does not change.

The system Cu(II)/**WT** has been explored also at the metal/ligand ratio of $(1.9:1)\cdot10^{-3}$ mol dm^{-3}. As expected, this favours the formation of binuclear species (see ESI-MS spectrum of Fig. S9, ESI†) where two Cu(II) ions are coordinated to the same peptide molecule (Fig. 1b). Under these experimental conditions, the complex $[Cu_2H_{-1}L]^+$, which is formed starting from pH 4, reaches a percentage of about 45%, being the predominant species around pH 5.5. It is reasonable to assume that, while one Cu(II) ion is coordinated to the N-terminal domain in the above described ATCUN mode, the second metal atom is bound to one of the two remaining histidines of the chain, with the possible participation of one or both the side carboxylate groups of Glu residues; the stoichiometry of this complex requires that the third histidine is still protonated. Available data do not allow to state if the "anchor" of the second Cu(II) ion is His-4 or His-8; a mixture of these two species is likely. In the pH range 5–8, the third histidine releases its proton, leading to the species $[Cu_2H_{-2}L]$, which dominates at pH 6–7. The corresponding pK_a value (5.52, Table 2) much lower than that measured in the absence of copper (6.96, Table 1), suggests that this His binds the second Cu(II) ion. Moving to alkaline pH, the species $[Cu_2H_{-4}L]^{2-}$ is formed: two protons are released in a quick sequence, probably corresponding to the deprotonation and coordination of two peptide nitrogens. A further deprotonation step is observed at the most alkaline pH values, characterized by a pK_a value of 9.04; it can be attributed to the coordination of a third amide nitrogen, which most likely substitutes one imidazole in the equatorial plane of the complex, leading to the formation of the species $[Cu_2H_{-5}L]^{3-}$, whose binding mode is $(N_{Im}, NH_2, 2N^-)(N_{Im}, 3N^-)$. In principle, both His-4 and His-8 can originate this binding mode, where the peptide wraps around the second Cu(II) ion through the coordination of the amide nitrogens of its peptide chain. The significant difference is that, if His-4 is bound to copper in the equatorial plane of the complex, the amide coordination should proceed in the C-terminal direction (due to the presence of the other complexed metal ion) while, in the case of His-8, it can proceed towards the N-terminus. It is well known in the literature that both these modes are possible, but the latter leads to more stable complexes than the former due to the different dimension of the formed chelation rings [35, 36].

Spectroscopic data (Figs. S7b and S8b; Table S2, SI†) confirm the above hypotheses. The two Vis absorption spectra recorded at pH 4.5 and 5.0, where the complex $[Cu_2H_{-1}L]^+$ is the prevailing species in solution, show two maxima: the first, more intense, at λ_{max} = 528 nm corresponds to the ATCUN coordination mode of the first Cu(II) ion. The second band, around λ_{max} = 740-730 nm, can be attributed to the coordination of an imidazole nitrogen to the second copper atom with the possible participation of the side carboxylate group of one Glu residue (expected absorption

maximum: 731 nm [32]). Increasing the pH, the second band shifts to shorter wavelengths, as a consequence of the coordination of further nitrogens to the second Cu(II) in the C-terminal domain of **WT**. At pH = 11, only one intense absorption band is observed at 520 nm, typical of a Cu(II) species where 3 amidic nitrogens of the peptide chain and one imidazole are bound to the equatorial plane of the complex (expected λ_{max} = 522 nm [32]). This is exactly the coordination mode suggested above for the second metal ion in the complex $[Cu_2H_{-5}L]^{3-}$. This band is superimposed to that of the ATCUN-type copper. EPR spectra recorded in the presence of excess of Cu(II) are very weak, confirming the formation of binuclear complexes. CD spectra (Fig. S8b and Table S2, SI†) at pH 5 are practically identical to those already described above for the solutions containing an excess of ligand and referring to the ATCUN-type complex. However, when the Cu(II) ion is instead in excess, increasing the pH value, the shape of CD spectra undergoes a dramatic change, due to the contribution of the second Cu(II) ion. The final spectrum, at pH 10.2, is very similar to that already previously reported for a Cu(II)/peptide binding mode (N_{Im}, $3N^-$) [37], attributable to the species $[Cu_2H_{-5}L]^{3-}$.

*MAAHEEQHG-Am (**H3A**)*

The thermodynamic complex-formation constants for the system Cu(II)/**H3A** are reported in Table 3 and the corresponding distribution diagrams are shown in Fig. 2.

Table 3. Cumulative complex-formation constants (β) and acid dissociation constants (K_a) of Cu(II) complexes with the peptide MAAHEEQHG-Am (**H3A)**, at T = 298.2 K and I = 0.1 mol dm^{-3} (KCl). Standard deviations on the last figure in parentheses.

Species	**log β**	**pK_a**
$[CuH_2L]^{2+}$	19.59(3)	4.93
$[CuHL]^{+}$	14.66(2)	5.62
[CuL]	9.04(3)	6.82
$[CuH_{-1}L]^{-}$	2.22(4)	7.30
$[CuH_{-2}L]^{2-}$	-5.08(5)	10.14
$[CuH_{-3}L]^{3-}$	-15.22(7)	-
$[Cu_2H_{-1}L]^{+}$	6.76(4)	-
$[Cu_2H_{-3}L]^{-}$	-6.53(4)	7.68
$[Cu_2H_{-4}L]^{-2}$	-14.21(6)	9.03
$[Cu_2H_{-5}L]^{-3}$	-23.24(7)	11.0
$[Cu_2H_{-6}L]^{-4}$	-34.2(1)	-

The **H3A** peptide is the only one, in the series here investigated, that does not have a histidine in third position: this definitively influences its ability to coordinate the Cu(II) ion, resulting in complexes which are significantly weaker than those formed by **WT** (over 3.5 orders of magnitude in the case of the species [CuL]). However, the presence of two histidines, separated by three amino acid residues, allows, also in this case, the formation of binuclear complexes, as demonstrated by the mass spectrum of Fig. S10b SI†, recorded in excess of metal.

The first species observed at acidic pH is the complex $[CuH_2L]^{2+}$, the main complex up to pH 5. Both its stoichiometry and the spectroscopic parameters (Figs. S11 and S12, Table S3, SI†) suggest that the metal is bound to the nitrogen of a histidine imidazole side chain, with the possible participation of the carboxylic group of a glutamic acid. Since the sequence contains two His and two Glu residues, it is likely a mixture of complexes in solution with this type of coordination but with different donor atoms involved. The loss of a proton leads to the formation of the $[CuHL]^{+}$ complex, which reaches its maximum at pH 5.5; the experimental value of λ_{max} is very close to that expected for a coordination ($2N_{Im}$, COO^-), with the formation of a macrochelate between the two histidines. The corresponding pK_a value (4.98), considerably lower than that measured for the second histidine in the absence of metal (6.77, Table 1), supports this coordination hypothesis.

a)

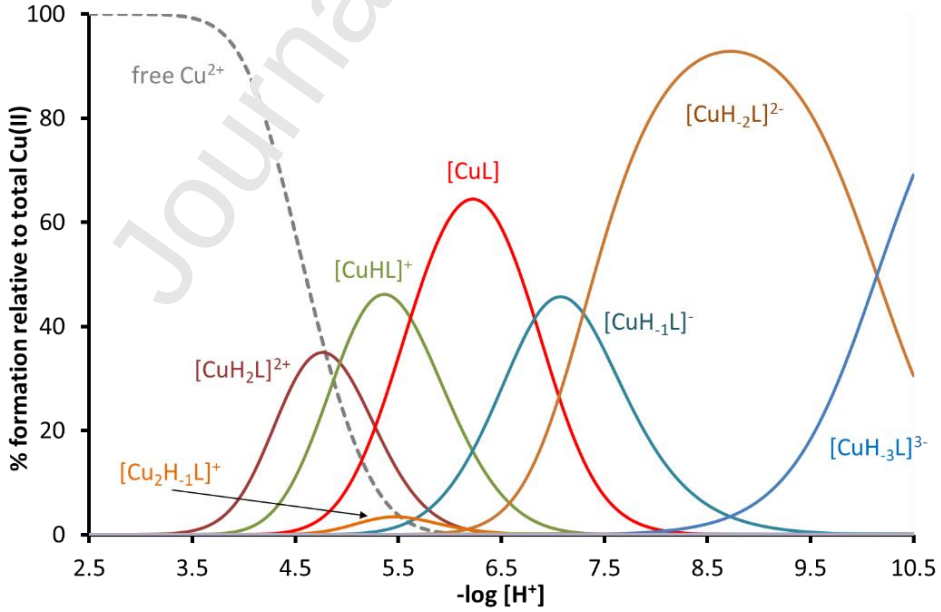

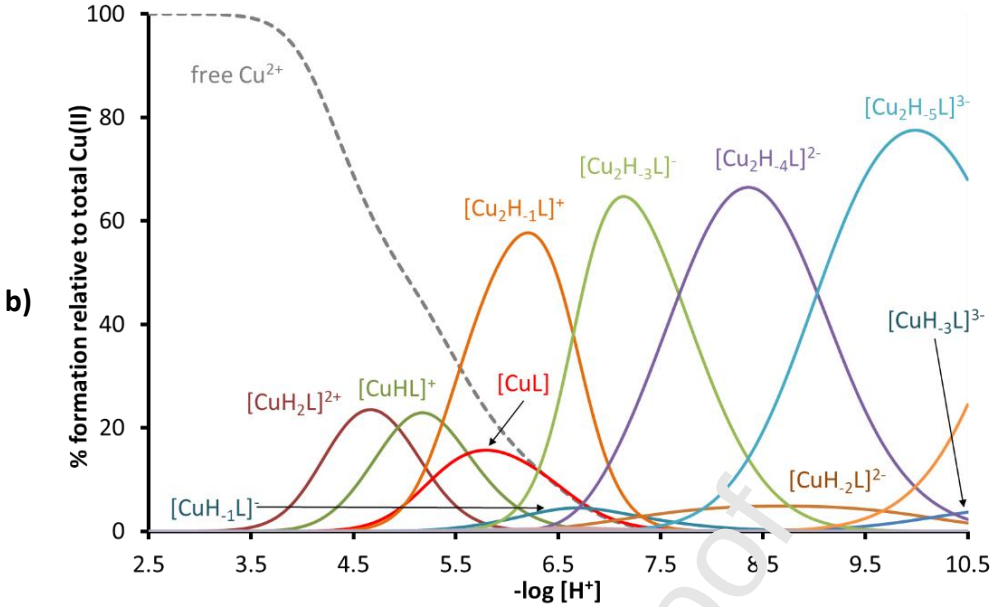

Fig. 2. Representative species distribution diagrams for complex-formation of **H3A** with Cu(II), at *T* = 25 °C and *I* = 0.1 mol dm^{-3} (KCl). $C_L = 1.0 \cdot 10^{-3}$ mol dm^{-3} and a) $C_{Cu(II)} = 0.8 \cdot 10^{-3}$ mol dm^{-3}; b) $C_{Cu(II)} = 1.9 \cdot 10^{-3}$ mol dm^{-3}.

Starting from pH 4.5, the formation of the complex [CuL] is observed (Fig. 2a). The thermodynamic and spectroscopic parameters suggest the deprotonation and coordination of the terminal amino group, which replaces an imidazole ring in the equatorial plane of the complex (N_{Im}, NH_2, COO^-); the fourth vertex of the plane is probably occupied by a water molecule, while the second imidazole ring becomes free or interacts with the metal in axial position. When, on the other hand, the metal ion is in excess, the binuclear complex $[Cu_2H_{-1}L]^+$ forms in a considerable amount, in parallel with [CuL]. Here, the additional metal ion is linked to the second histidine and to an amide nitrogen of the peptide chain. Both the complex [CuL] and the species $[Cu_2H_{-1}L]^+$, have their formation maximum around pH 6. As pH increases, each metal ion anchored to the peptide is able to gradually displace the amide protons of the chain, thus binding the corresponding amide nitrogens. The wavelength of maximum absorption in the Vis spectra shifts to lower values as the pH increases: the absorption band is narrower and more intense when only mononuclear complexes are present (with a unique and well-defined coordination site) while it is broader for binuclear complexes that contain two similar but not identical metal-binding sites. The CD spectra (Fig. S12, SI†) have very similar shapes, especially in their UV portion, confirming that the type of donor atoms is the same in the two cases.

*MAHAEEQHG-Am (**H4A**)*

The thermodynamic complex-formation constants for the system Cu(II)/**H4A** are reported in Table 4 and the corresponding distribution diagrams are shown in Fig. 3.

Table 4. Cumulative complex-formation constants (β) and acid dissociation constants (K_a) of Cu(II) complexes with the peptide MAHAEEQHG-Am (**H4A)**, at T = 298.2 K and I = 0.1 mol dm^{-3} (KCl). Standard deviations on the last figure in parentheses.

Species	**log β**	**pK_a**
$[CuHL]^{+}$	15.15(3)	4.60
[CuL]	10.55(3)	4.71
$[CuH_{-1}L]^{-}$	5.84(2)	6.83
$[CuH_{-2}L]^{2-}$	-0.99(4)	-
$[Cu_2H_{-1}L]^{+}$	8.74(5)	5.76
$[Cu_2H_{-2}L]$	2.98(7)	6.56
$[Cu_2H_{-3}L]^{-}$	-3.58(7)	6.34
$[Cu_2H_{-4}L]^{-2}$	-9.92(3)	8.88
$[Cu_2H_{-5}L]^{-3}$	-18.80(4)	-

The replacement of histidine in position 4 with an alanine does not preclude the peptide **H4A** from complexing Cu(II) as described above for **WT**: in fact, His in third position leads to the formation of the stable ATCUN-type complexes, while the presence of a second histidine in position 8 allows the formation of binuclear complexes. The presence of the latter species, detected by potentiometry, was confirmed by the mass spectra recorded in excess of metal (Fig. S13, SI†). The speciation model of Table 4 does not differ very much from that determined for the **WT** peptide (Table 2) except for the absence of the most protonated species $[CuH_3L]^{3+}$ and $[CuH_2L]^{2+}$; this is obviously due to the lack of one histidine residue. In excess of ligand, the ATCUN-type complex, with stoichiometry $[CuH_{-1}L]^{-}$, is already the predominant species at pH 5; at alkaline pH, the second histidine releases the proton bound to the pyridine-type nitrogen of its imidazole ring, with a pK_a value (6.83) very similar to that measured in the absence of metal (6.88), thus suggesting the absence of any interaction with the Cu(II) ion already bound to the N-terminal domain. The Vis-absorption (Fig. S14a, SI†) and the CD spectra (Fig. S15a, SI†) confirm this coordination hypothesis, since they are practically unchanged throughout the explored pH range (Table S5, SI†). Interestingly, although the replacement of His in position 4 with Ala does not

change the peptide coordination modes, the mono-nuclear complexes of **WT** are more stable than those formed by **H4A** (see competition diagrams discussed below). This result is in agreement with the observation, already widely documented in the literature, that the number of histidine residues of the peptide sequence always has a great influence on the stability of the formed Cu(II) complexes, due to the possibility of forming a number of species with the same stoichiometry but a different set of donor atoms. Lastly, in the presence of metal excess, the spectroscopic data (Figs. S14b and S15b, Table S6, SI†) have a very similar trend to that already discussed above for **WT**, confirming the formation of binuclear species with similar structure and stability of those already described for **WT**.

a)

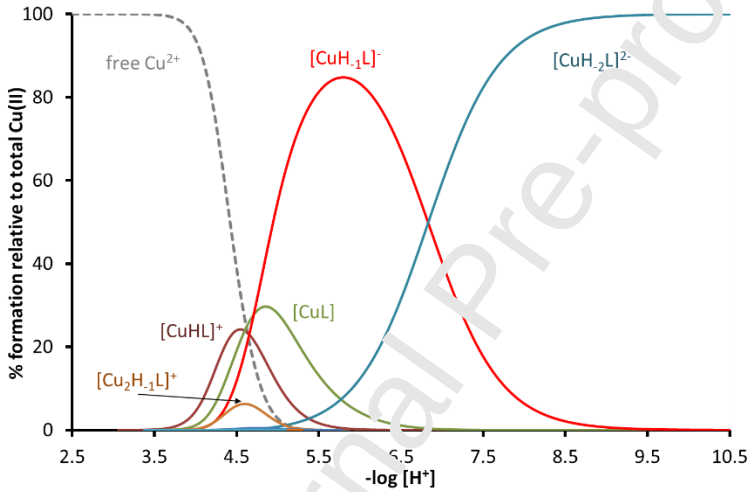

b)

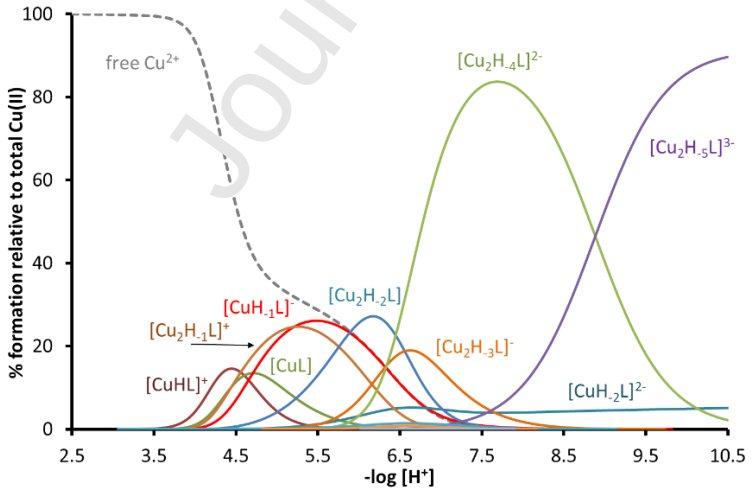

Fig. 3. Representative species distribution diagrams for complex-formation of **H4A** with Cu(II), at T = 25 °C and I = 0.1 mol dm^{-3} (KCl). C_L = 1.0·10^{-3} mol dm^{-3} and a) $C_{Cu(II)}$ = 0.8·10^{-3} mol dm^{-3}; b) $C_{Cu(II)}$ = 1.9·10^{-3} mol dm^{-3}.

*MAHHEEQAG-Am (**H8A**)*

The thermodynamic complex-formation constants for the system Cu(II)/**H8A** are reported in Table 5 and the corresponding distribution diagrams are shown in Fig. 4.

Table 5. Cumulative complex-formation constants (β) and acid dissociation constants (K_a) of Cu(II) complexes with the peptide MAHHEEQAG-Am (**H8A)**, at T = 298.2 K and I = 0.1 mol dm^{-3} (KCl). Standard deviations on the last figure in parentheses.

Species	**log β**	**pK_a**
$[CuH_2L]^{2+}$	19.33(2)	-
[CuL]	10.55(1)	4.87
$[CuH_{-1}L]^{-}$	5.68(2)	6.76
$[CuH_{-2}L]^{2-}$	-1.08(4)	-
$[Cu_2H_{-1}L]^{+}$	8.82(5)	5.82
$[Cu_2H_{-2}L]$	3.00(7)	-
$[Cu_2H_{-4}L]^{-2}$	13.12(3)	9.32
$[Cu_2H_{-5}L]^{-3}$	-22.44(4)	-

The **H8A** peptide contains two histidine residues which, although close together, can lead to the formation of binuclear species. A first metal ion is bound by the N-terminal ATCUN site, starting from pH 3, and this complex (variously protonated depending on pH) is practically the only species in solution in the presence of ligand excess. If, on the other hand, the metal is in excess, a second Cu(II) ion can first anchor to the histidine in position 4 and then bind, at basic pH, the amides of the peptide backbone in the C-terminal direction. The formation of binuclear complexes, suggested by the potentiometric results of Table 5, is confirmed by the mass spectra, an example of which is shown in Fig. S16 SI†). The spectrophotometric results confirm a behaviour similar to that of the other peptides (Figs. S17 and S18, Tables S7 and S8, SI†). It is worth of note that two consecutive histidines really do give rise to binuclear complexes.

a)

b)

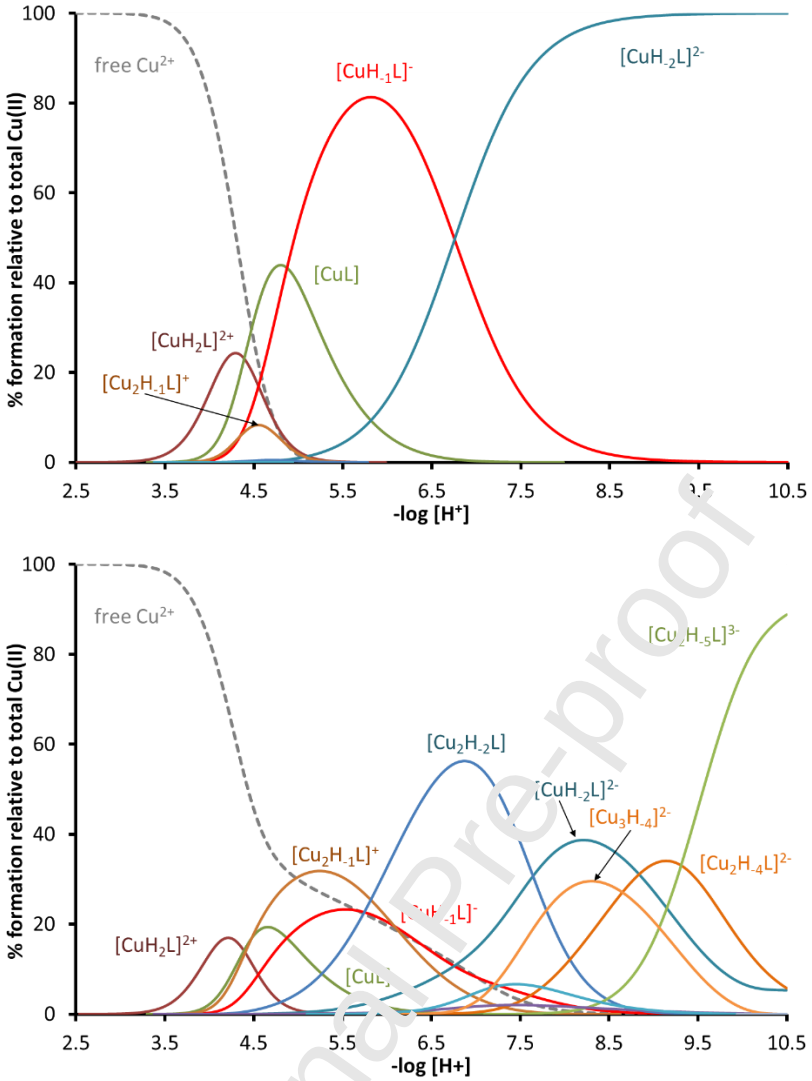

Fig. 4. Representative species distribution diagrams for complex-formation of **H8A** with Cu(II), at T = 25 °C and I = 0.1 mol dm^{-3} (KCl). C_L = 1.0·10^{-3} mol dm^{-3} and a) $C_{Cu(II)}$ = 0.8·10^{-3} mol dm^{-3}; b) $C_{Cu(II)}$ = 1.9·10^{-3} mol dm^{-3}.

*MAHAEEQAG-Am (**H4A/H8A**)*

Table 6. Cumulative complex-formation constants (β) and acid dissociation constants (K_a) of Cu(II) complexes with the peptide MAHAEEQAG-Am (**H4A/H8A)**, at T = 298.2 K and I = 0.1 mol dm^{-3} (KCl). Standard deviations on the last figure in parentheses.

Species	**log β**	**pK_a**
$[CuHL]^{+}$	12.95(1)	-
$[CuH_{-1}L]^{-}$	4.27(1)	5.28
$[CuH_{-2}L]^{2-}$	-0.99(1)	-

The thermodynamic complex-formation constants for the system Cu(II)/MAHAEEQAG-Am (**H4A/H8A**), are reported in Table 6 and the corresponding distribution diagram is shown in Fig. 5.

Only the histidine in third position is present in this peptide and, therefore, only mononuclear, ATCUN-type complexes are formed in the explored pH range. In addition, Vis absorption data (Fig. S19, Table S9, SI†) show that, in the presence of Cu(II) excess, the solution becomes cloudy at pH > 7 for the formation of a precipitate, most likely of Cu(II) hydroxide. CD spectra (Fig. S20, Table S9, SI†) are almost identical at 0.8:1.0 and 1.9:1.0 metal-to-ligand ratios, supporting the absence of polynuclear complexes.

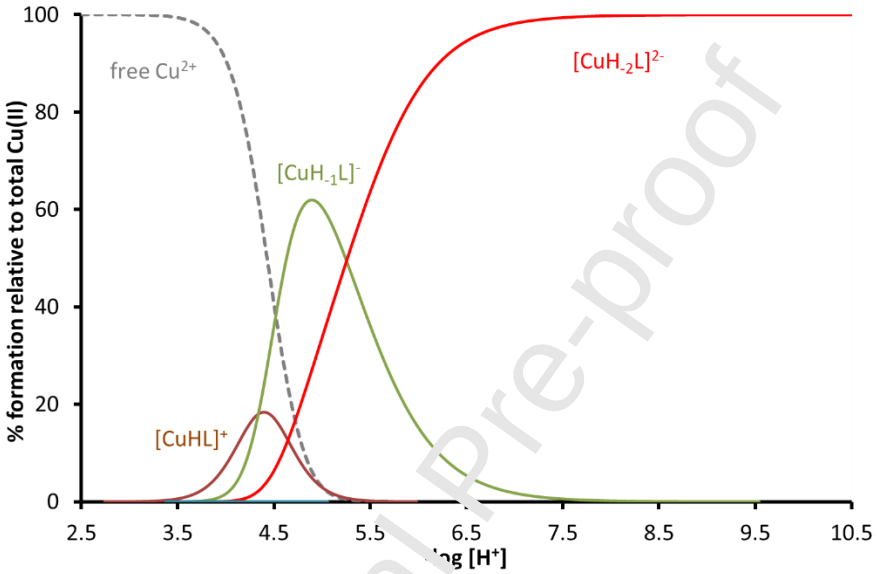

Fig. 5. Representative species distribution diagram for complex-formation of **H4A/H8A** with Cu(II), at T = 25 °C and I = 0.1 mol dm^{-3} (KCl). C_L = 1.0·10^{-3} mol dm^{-3} and $C_{Cu(II)}$ = 0.8·10^{-3} mol dm^{-3}.

Binary Ni(II) complexes

The complex-formation equilibria with the Ni(II) ion have been investigated only in the presence of ligand excess and only mono-nuclear complexes have been detected. The speciation models obtained by potentiometry are shown in Table 7, while the corresponding distribution diagrams and all the spectroscopic results are reported as SI† (Figs. S22-S41, Tables S10–S14). The formation of yellow, diamagnetic, square-planar complexes has been observed at alkaline pH in every system, with a slow kinetics which required rather long waiting times between each titrant addition. No precipitation was observed in the explored pH range.

The presence of the ATCUN type sequence in all peptides, with the exception of **H3A**, favours the Ni(II) coordination to the amino-terminal domain, as already described for copper. The

main species at neutral pH is the (N_{Im}, NH_2, $2N^-$) complex, characterized by an intense absorption around 422 nm [20, 38]; the corresponding CD spectrum contains, in the Vis range, two bands of opposite sign, at 415 (positive) and 480 (negative) nm, respectively [39-41], and a positive and intense charge-transfer band in the UV region around 260 nm [42, 43]. However, it should be noted that the shape of CD spectra referring to the peptides **WT** and **H4A** progressively changes at pH>9, although no variations are observed either in the absorption spectra or in the distribution diagrams (where the complex $[NiH_{-2}L]^{2-}$ is practically the only species detected in solution at pH> 8). On the contrary, for the **H8A** and **H4A/H8A** peptides, in which the histidine in position 8 has been replaced by an alanine, the CD spectrum simply becomes more intense, as pH increases, without changing shape. Evidently, His-8, when present, is somehow involved in coordination at high pH, for example with a shift of nickel from the N-terminal to the C-terminal domain. However, the available experimental data are not enough to fully clarify this point, which would require further investigation.

A peculiar behaviour is that of **H3A**, due to the lack of the ATCUN-type coordination domain. Likely, at acidic pH, the Ni(II) ion is anchored to one His residue [38, 44] and then, as pH increases, macrochelated species are formed, with the involvement of the second histidine and/or of the terminal amino group. The species formed at acidic pH are probably octahedral; they evolve to the classical square planar, low spin complex at alkaline pH, with the involvement of deprotonated amide nitrogens of the backbone. As a matter of fact, up to four deprotonation steps are revealed by potentiometry at alkaline pH, suggesting the coordination of more than two amide nitrogens to Ni(II). This behaviour is confirmed by spectroscopic data (Figs. S28 and S29, SI†): the wavelength of maximum absorption at pH > 10 is 414 nm, lower than that recorded for the other systems (about 422 nm). In addition, the CD spectra in the Vis range show a single broad and intense negative band, located around 440 nm.

Table 7. Cumulative complex-formation constants (β) and acid dissociation constants (K_a) of Ni(II) complexes with the investigated peptides, at T = 298.2 K and I = 0.1 mol dm^{-3} (KCl). Standard deviations on the last figure in parentheses.

Ligand	Species	log β	pK_a
MAHHEEQHG-Am (wild-type, **WT**)	$[NiHL]^+$	12.90(8)	5.77
	[NiL]	7.13(6)	6.26
	$[NiH_{-1}L]^-$	0.87(5)	6.95
	$[NiH_{-2}L]^{2-}$	-6.08(5)	-

MAAHEEQHG-Am (**H3A**)	$[NiH_2L]^{2+}$	18.0(2)	6.0
	$[NiHL]^{+}$	11.98(8)	6.25
	[NiL]	5.73(6)	7.78
	$[NiH_{-1}L]^{-}$	-2.05(8)	-
	$[NiH_{-3}L]^{3-}$	-18.64(7)	9.1
	$[NiH_{-4}L]^{4-}$	-27.7(1)	-
MAHAEEQHG-Am (**H4A**)	[NiL]	6.25(8)	5.49
	$[NiH_{-1}L]^{-}$	0.76(2)	6.89
	$[NiH_{-2}L]^{2-}$	-6.13(5)	-
MAHHEEQAG-Am (**H8A**)	[NiL]	6.01(6)	5.75
	$[NiH_{-1}L]^{-}$	0.26(3)	6.72
	$[NiH_{-2}L]^{2-}$	-6.46(4)	-
MAHAEEQAG-Am (**H4A/H8A**)	$[NiH_{-1}L]^{-}$	-0.48(5)	5.55
	$[NiH_{-2}L]^{2-}$	-6.03(1)	-

Binary Zn(II) complexes

The Zn(II) ion has a strong affinity for the imidazole nitrogen of histidine, while it is generally accepted that it is not able to displace the protons of the amide nitrogens. In all the studied systems, the formation of 1:1 complexes, variously protonated, was observed (see Table 8, distribution diagrams of Figs. S42–S46 SI† and mass spectra of Figs. S47–S51 SI†). The first complexes are formed in all systems starting from pH 4.5 – 5.5: the stoichiometry of these species depends on the number of histidines in the sequence ($[ZnH_2L]^{2+}$ in the case of **WT**; $[ZnHL]^{+}$ in the case of **H3A**, **H4A** and **H8A**; [ZnL] in the case of **H4A/H8A**). In every case, the stoichiometry requires that two nitrogen atoms are unprotonated and bound to the metal. They should belong to the two available imidazole side chains; or, in the case of **H4A/H8A**, to the histidine and the terminal amino group. It should be noted that, in the case of **WT**, which contains three histidines, a mixture of complexes, with identical stoichiometry and coordination mode but involving different donor atoms, can be formed. This may explain why the $[ZnH_2L]^{2+}$ complex of **WT** begins to form at a pH value (4.5) lower than that observed with the other peptides. It is also worth noting that, when the histidine in position 8 is replaced by an alanine (peptides **H8A** and **H4A/H8A**) the first complexes are formed only at pH around 5.5, suggesting an important role of

His-8 as the first metal anchor. All these complexes should be macrochelated, most likely with a tetrahedral geometry, where the two coordination positions not occupied by nitrogens are occupied by water molecules. As the pH increases, the third nitrogen of the peptide, if present, binds the metal by displacing a water molecule. Only in the case of **WT**, zinc can simultaneously coordinate three histidine residues. In addition, also the formation of a species with four nitrogen atoms linked to zinc is theoretically possible for **WT,** corresponding to the complex [ZnL]; this could be the reason for its greater stability (almost two orders of magnitude) compared to the other complexes of the same stoichiometry formed by the other peptides (see Table 8). Unexpectedly, the solutions containing Zn(II) and **WT** are the only ones in which the formation of a precipitate was observed between pH 7 and 10.2. In all other cases, no clouding of the solution was detected, although the potentiometric signal had a slow drift at pH> 8.5. At alkaline pH, further deprotonation steps have been observed, which lead to the formation of the species $[ZnH_{-1}L]^-$ and, only in the case of **H4A/H8A**, also $[ZnH_{-2}L]^{2-}$. The simplest explanation is the deprotonation of the coordinated water molecules.

Table 8. Cumulative complex-formation constants (β) and acid dissociation constants (K_a) of Zn(II) complexes with the investigated peptides, at T = 298.2 K and I = 0.1 mol dm^{-3} (KCl). Standard deviations on the last figure in parentheses.

Ligand	Species	log β	pK_a
MAHHEEQHG-Am (wild-type, **WT**)	$[ZnH_2L]^{2+}$	18.79(6)	6.23
	$[ZnHL]^{+}$	12.56(6)	6.46
	[ZnL]	6.10(4)	-
MAAHEEQHG-Am (**H3A**)	$[ZnHL]^{+}$	11.71(4)	6.93
	[ZnL]	4.78(4)	8.02
	$[ZnH_{-1}L]^{-}$	-3.24(5)	-
MAHAEEQHG-Am (**H4A**)	$[ZnHL]^{+}$	11.69(3)	7.22
	[ZnL]	4.47(6)	8.37
	$[ZnH_{-1}L]^{-}$	-3.9(1)	-
MAHHEEQAG-Am (**H8A**)	$[ZnHL]^{+}$	10.71(6)	6.58
	[ZnL]	4.13(3)	8.23
	$[ZnH_{-1}L]^{-}$	-4.10(4)	-
MAHAEEQAG-Am (**H4A/H8A**)	[ZnL]	3.88(6)	7.84
	$[ZnH_{-1}L]^{-}$	-3.96(6)	8.46

$[ZnH_{-2}L]^{2-}$	-12.42(6)	-

Ternary Cu(II)/Ni(II)/WT complexes

Data reported above show that, in the presence of Cu(II) excess, the **WT** peptide can form binuclear species. Therefore, we decided to test its behavior in the presence of equimolar quantities of Cu(II) and Ni(II). First, from a qualitative point of view, it was possible to observe, during the titrations with KOH, that the solution, initially colorless, assumed a pink color at acidic pH close to neutrality and then turned to orange at basic pH.

Potentiometric data processing revealed the formation of three hetero-metallic binuclear species, as reported in Table 9; the corresponding distribution diagram is shown in Fig. 6. This result is in excellent agreement with a recent study carried out under similar conditions on the AAHAAAHG octapeptide [45]. Although that paper does not report the complex-formation constants of the mixed species, the stoichiometry of the ternary complex formed at basic pH, obtained from mass spectra, is exactly $[CuNiH_{-5}L]^{3-}$, which corresponds (except for the different charge due to the different number of carboxylic groups of the sequence) to that obtained in the present investigation. Furthermore, the absorption spectra shown in Fig. 7 are very similar to those reported by Grenacs et al. [45] suggesting the same coordination geometry. Therefore, it can be assumed that, at acidic pH, Cu(II) coordinates at the N-terminus of **WT** (with the ATCUN-type coordination mode); as pH is increased, a nickel ion initially binds the two histidine residues not involved in copper coordination. Starting from pH about 9, the Ni(II) ion displaces up to 3 amide hydrogens of the peptide chain, thus forming the classic planar and diamagnetic 4N complex. It is reasonable to assume that, in the species $[CuNiH_{-5}L]^{3-}$ (which dominates at pH> 9, see Fig. 6) the Ni(II) ion is bound to His-8 and to the three preceding amides, in the N-terminal direction. In the pH range 4-5 – 8.5, the absorption spectra are practically identical and dominated by the d-d transition of the Cu(II) ATCUN-type complex; at more alkaline pH values, the typical band of the diamagnetic Ni(II) complex becomes instead evident.

ESI-MS spectra recorded at pH 5.5, 7.8 and 10.2 (Fig. S52 SI†) also highlight the formation of binuclear complexes with Cu(II) and Ni(II) at different protonation states and they are in good agreement with the speciation model obtained by potentiometry. Following the distribution diagram plotted in Figure 6, the observed more intense m/z signals correspond to the major species in solution under the given pH.

Table 9. Cumulative complex-formation constants (β) and acid dissociation constants (K_a) of mixed Cu(II)/Ni(II) complexes with peptide **WT**, at T = 298.2 K and I = 0.1 mol dm^{-3} (KCl). Standard deviations on the last figure in parentheses.

Species	**log β**	**pK_a**
$[CuNiH_{-1}L]^{+}$	9.97(6)	6.57
$[CuNiH_{-2}L]$	3.40(4)	-
$[CuNiH_{-5}L]^{3-}$	-23.74(4)	-

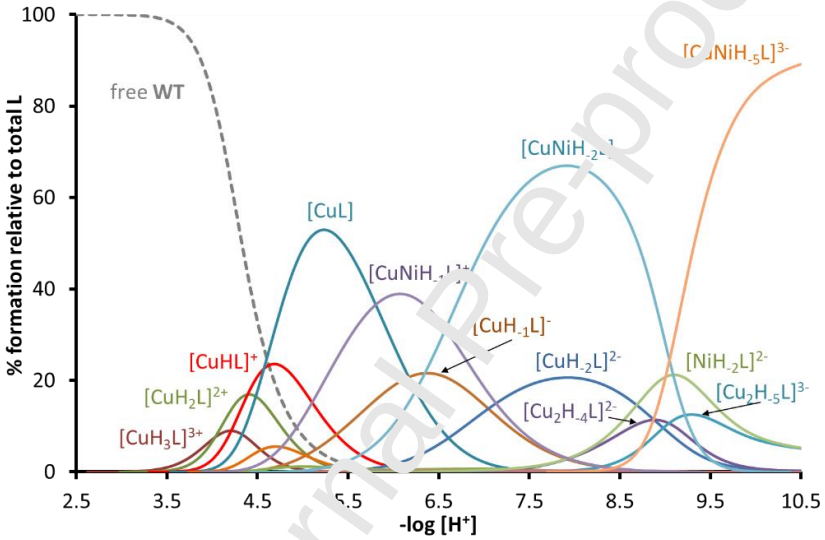

Fig. 6. Representative species distribution diagram for complex-formation in the ternary Cu(II)/Ni(II)/**WT** system, at T = 25 °C and I = 0.1 mol dm^{-3} (KCl). C_L = $C_{Cu(II)}$ = $C_{Ni(II)}$ = 1.0·10^{-3} mol dm^{-3}.

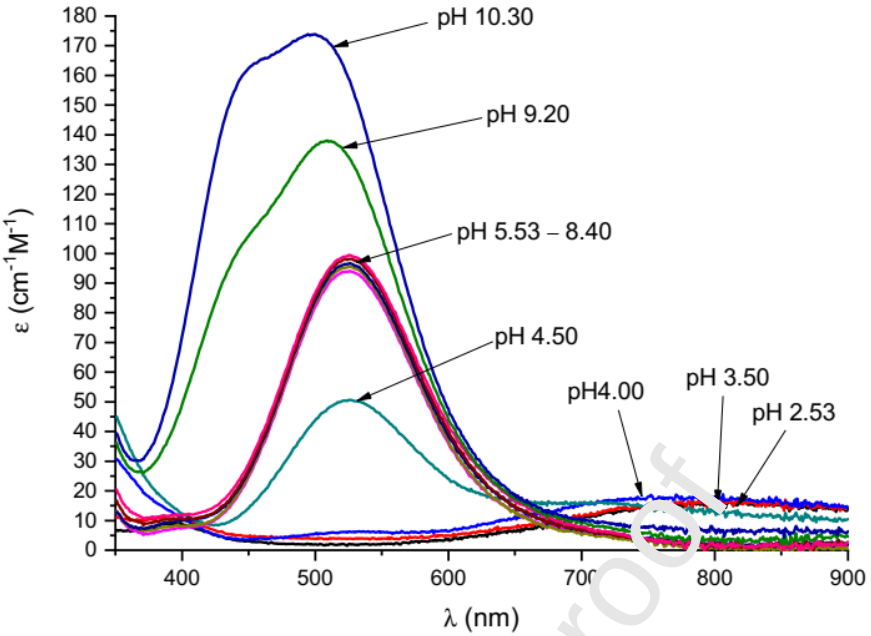

Fig. 7. Vis absorption spectra for Cu(II)/Ni(II) complexes with **WT**; C_L = 1.0·10^{-3} mol dm^{-3}, Cu(II):L = 0.8 : 1, Ni(II):L = 0.9 : 1.

Comparison of complex stability

When the various histidines of a peptide sequence have very similar chemical environments, spectroscopic techniques are unable to distinguish the behavior of each specific residue. Hence the need to study series of analogues, e.g. with the Ala-scan method used here. To obtain the required information, the stability of the complexes formed by the different mutants must be compared; however, this cannot be directly done through the stability constants, since the complexes have different stoichiometry and/or protonation degree. For this purpose, the parameters reported in Tables 10-12 have been calculated. The general meaning of these parameters is to give an overall estimation of the metal-ligand "affinity", under well-defined experimental conditions of pH and component concentration, which summarizes all the metal-ligand interactions that give rise to the speciation models described above. In particular, K_d (expressed as molarity, mol dm^{-3}) corresponds to the concentration of free metal when the ligand is half in the form of a complex (whatever its stoichiometry) and half not complexed [46]. K_d depends on pH but not on the ligand concentration and the smaller it is, the greater the complexes stability is. This parameter is widely used in biochemistry, assuming that, if the K_d value is equal to or less than the free metal concentration estimated (or measured) in the biological environment, then the ligand can "capture" the metal. A similar meaning can also be attributed to

pM (= -log[M]$_{free}$); in this case a higher value means that the ligand is more effective in metal sequestration [47]. The parameter $pL_{0.5}$, recently introduced by Sammartano and coworkers [48], refers to the quantity of ligand (expressed as -log[L]$_{tot}$) required to bind 50% of the metal present in traces (typically $[M]_{tot} = 1 \cdot 10^{-12}$ mol dm^{-3}). This parameter takes into account the action of all the other possible competing ligands present in solution (the speciation model of which must be known) and it is the greater the smaller the quantity of ligand required, i.e. the stronger the metal-ligand affinity. The values of K_d, pM and $pL_{0.5}$, at different pH and for all the systems studied are shown in Tables 10-12 together with reference values for the tetrapeptide DAHK-Am, corresponding to the ATCUN site of human albumin.

Table 10. Calculated dissociation constants (K_d/ mol dm^{-3}), pM and $pL_{0.5}$ values for Cu(II) complexes with the investigated peptides.

	K_d[(a)]		pCu[(b)]		$pL_{0.5}$[(c)]	
	pH = 7.4	**pH = 5.4**	**pH = 7.4**	**pH = 5.4**	**pH = 7.4**	**pH = 5.4**
WT	$2.35 \cdot 10^{-14}$	$9.95 \cdot 10^{-8}$	14.408	7.959	12.27	7.00
H3A	$4.03 \cdot 10^{-10}$	$1.65 \cdot 10^{-5}$	10.173	6.198	9.23	4.59
H4A	$4.48 \cdot 10^{-14}$	$2.26 \cdot 10^{-7}$	14.128	7.610	12.25	6.64
H8A	$4.63 \cdot 10^{-14}$	$1.31 \cdot 10^{-7}$	14.113	7.841	12.24	6.88
H4A/H8A	$4.26 \cdot 10^{-14}$	$2.52 \cdot 10^{-7}$	14.150	7.565	12.25	6.60
DAHK-Am[(d)]	$1.69 \cdot 10^{-14}$	$7.30 \cdot 10^{-8}$	14.550	8.093	12.28	7.14

[(a)] Kozlowski et al. [46]
[(b)] $[L]_{total} = 10^{-5}$ M and $[M]_{total} = 10^{-6}$ M; Crisponi et al. [47]
[(c)] Crea et al. [48]
[(d)] Speciation model taken from: Sokolowska et al. [40]

Table 11. Calculated dissociation constants (K_d/ mol dm^{-3}), pM and $pL_{0.5}$ values for Ni(II) complexes with the investigated peptides, at pH = 7.4.

	K_d	pNi	$pL_{0.5}$
WT	$6.19 \cdot 10^{-9}$	9.163	8.21
H3A	$5.24 \cdot 10^{-6}$	6.444	5.28
H4A	$5.89 \cdot 10^{-9}$	9.184	8.23
H8A	$1.13 \cdot 10^{-8}$	8.901	7.95
H4A/H8A	$4.72 \cdot 10^{-9}$	9.281	8.33
DAHK-Am[(d)]	$1.85 \cdot 10^{-9}$	9.689	8.73

[(d)] Speciation model taken from: Sokolowska et al. [40]

Table 12. Calculated dissociation constants (K_d/ mol dm^{-3}), pM and $pL_{0.5}$ values for Zn(II) complexes with the investigated peptides, at pH = 7.4.

	K_d	pZn	$pL_{0.5}$
WT	$3.17 \cdot 10^{-6}$	6.582	5.49
H3A	$4.44 \cdot 10^{-5}$	6.084	4.34
H4A	$6.99 \cdot 10^{-5}$	6.056	4.14
H8A	$1.70 \cdot 10^{-4}$	6.024	3.76
H4A/H8A	$2.65 \cdot 10^{-4}$	6.016	3.56

As for the Cu(II) complexes, from Table 10 it is clear that the best ligand in the series is human albumin at both pH 7.4 and 5.4: although the coordination site is always of the ATCUN type and therefore the binding mode is very similar for all peptides (with the exception of **H3A**), the particular albumin sequence is favored probably due to the presence of the aspartic acid residue, whose side carboxyl group can participate in the metal complexation through an axial interaction [49, 50]. In the series of Hpn protein analogues, **WT** forms the most stable complexes: the presence of an extra histidine residue and the possibility of forming different complexes with identical stoichiometry but different set of donor atoms is probably the reason of this greater affinity. The differences between the **H4A**, **H8A** and **H4A/H8A** ligands, which have an identical ATCUN site but different combinations of additional histidines, are of minor importance, although it can be observed that the **H4A/H8A** peptide, which only possesses one histidine in position 3 (and which consequently cannot form binuclear complexes), has the lowest affinity. A significantly lower strength as Cu(II) ligand is shown by **H3A**, where the histidine in position 3, responsible for the ATCUN sequence, was replaced by alanine. As expected, the His-3 residue is crucial to confer high Cu(II) binding affinity to the studied peptides like in human albumin. Similar considerations can be deduced from the competition diagram reported as Supplementary Material (Fig. S53, SI†), which allow to compare the strength of the ligands in a wide pH range.

Also in the case of Ni(II) complexes, the best ligand proved to be DAHK-Am (Table 11). Surprisingly, the peptide of the series which has the second-best affinity for Ni(II) is **H4A/H8A**, which contains less histidines than all the others. Evidently, the ATCUN binding motif, which leads to the formation of strictly square-planar Ni(II) complexes plays a major role and the presence of additional histidines is negligible, or even disturbing, when moving towards neutral and alkaline pH, as it can be observed from the competition diagram of Fig. S54, SI†. On the other hand, His-8

(which is absent in **H8A**) seems to contribute to the stability of the system; moreover, as discussed in the previous section, the obtained CD data for **WT** and **H4A** undergo a shape variation at pH > 9, suggesting that His-8 is somehow involved in coordination at alkaline pH. Once again, the lack of the His residue in position 3 strongly penalizes the **H3A** peptide, as already observed in the case of Cu(II).

The coordination modes of the Zn(II) ion are very different from those of Cu(II) and Ni(II), as described above. In this case, the number of histidine residues of the peptide plays a major role in establishing its affinity towards the metal. The results reported in Table 12 and Fig. S55 SI† show that **WT** is by far the strongest ligand of the series, at acidic pH; it is the only one which can form Zn(II) complexes with three imidazole nitrogens as donor atoms. In contrast, **H4A/H8A** is the weakest ligand; in fact, it possesses only one histidine. Moreover, the zinc affinity is significantly lower for the **H3A** and **H8A** peptides than for the **H4A** ligand, although all the three of them possess two histidines. This result suggests a minor role for His-4, with respect to His-3 and His-8, in zinc chelation.

Finally, the data of Tables 10-12 clearly show that, under the same experimental conditions, the N-terminal domain of Hpn (represented by **WT**) has great selectivity towards the metals studied with affinities in the following order: Cu(II) >> Ni(II) > Zn(II). Similar considerations also apply to the other peptides. As already described above, a recent study [13] reported, in the case of Ni(II), a K_d value for the Hpn protein of $7.89 \cdot 10^{-8}$. It can be considered in a reasonably good agreement with the value measured in the present work for the Ni(II)/**WT** system ($6.19 \cdot 10^{-9}$ M, Table 11), also taking into account that the experimental conditions are rather different. Hence, it can be deduced that the amino-terminal ATCUN site of Hpn plays an important role in the nickel coordination. On the contrary, in the case of Zn(II), the K_d value measured here for the peptide **WT** ($3.17 \cdot 10^{-6}$ mol dm^{-3}, Table 12) is much higher than that reported by Wegner et al. for the Hpn protein ($1.03 \cdot 10^{-9}$ mol dm^{-3}). This is attributable to the fact that Hpn has other binding sites rich in histidine and cysteine residues which have a greater affinity for zinc than the amino-terminal domain.

Conclusions

The studied peptides proved to be good chelators for divalent copper, nickel and zinc ions. With the exception of **H3A**, all the investigated sequences contain a very efficient Cu(II) and Ni(II)

ATCUN-binding site (N_{Im}, NH_2, $2N^-$) which is confirmed to confer great stability to copper and nickel complexes. Furthermore, the presence of additional histidines in position 4 and 8 allows the formation of stable homo- and hetero- binuclear complexes. In the case of Zn(II) ion, the ligand effectiveness is not strictly affected by the presence of the ATCUN sequence, but most likely depends on the number of available histidines, which act as multiple metal anchoring sites and allow the formation of macrochelate systems. The binding strength of the N-terminus of Hpn protein has been compared with that of the other studied binding sites of Hpn, i.e the two motifs containing a double cysteine residue in the positions 38–42 and 51–55 [17] and the poly-histidine sequence in the positions 18–26 [14]. The corresponding competition diagrams are reported as Supplementary Information (Figs. S56, S57 SI†). The -Cys-Cys- motifs are stronger than the N-terminal ATCUN site, both for Ni(II) and Zn(II) coordination. On the other hand, the poly-His sequence corresponding to the 18-26 domain of Hpn can compete with the N-terminus only at acidic pH value. In view of the fact that Hpn can bind up to five Ni(II) ions, we can suggest that all these four studied binding sites are involved in nickel trafficking. It looks reasonable that, at low nickel levels, the cysteine binding sites are saturated with nickel before than His binding sites.

The formation of binuclear Cu(II) complexes have been extensively studied; from the obtained results one can generally assume that the first Cu(II) ion interacts with the peptide at the very effective N-terminal ATCUN site (if present), while a second Cu(II) ion can further coordinate the histidine residues in position 4 and 8. However, His-8 seems to be the favorite site, due to the possibility to further coordinate the amide nitrogen towards the N-terminal direction, forming a stable 5/6-membered chelate rings.

As expected from the Irving-Williams series [51], the N-terminal domain of Hpn displays metal-binding affinities in the order Zn(II) < Ni(II) << Cu(II). In particular, this means that Cu(II), even if present in low amount, can replace Ni(II) in the Hpn protein coordination. Moreover, the **WT** model peptide was proved to form hetero-binuclear complexes, where the ATCUN sequence interacts exclusively with Cu(II) while nickel preferentially binds the histidine residue in position 8 (second binding site) to form its typical square planar complex (N_{Im}, $3N^-$)(see Fig. 8). In the interaction of Cu(II) with a binary Ni(II)/**WT** complex, the nickel ion can be either released or even moved from the ATCUN site to the second binding site. In both cases the activity of Hpn protein is disturbed. In fact, Figs. S58, S59 SI† show that, in the presence of only a 20% of Cu(II) with respect to Ni(II), not only mixed Cu(II)/Ni(II) species are formed in the entire pH range, but, at neutral pH, some Ni(II) is still not complexed (see Fig. S23 SI† for the sake of comparison in the absence of

copper). When thinking about possible antimicrobial strategies, a suitable Cu(II) complex, sufficiently stable to reach the bacterium but weaker that that formed with Hpn, could be employed as a pharmacophore, with the aim of producing a "ligand exchange" reaction, where Cu(II) ions substitute Ni(II) ions at the Hpn ATCUN domain; in a possible additional second step, the released Ni(II) ions could even be sequestered by the metal-free pharmacophore and eliminated. This action would partially inhibit the Hpn efficiency in Ni(II) recruitment and storage, thus helping the nutritional immunity mechanism to starve the pathogen. A similar action could also be obtained with the more safe Zn(II) ion, but it would require very high Zn(II) concentration, since its affinity for Hpn, at least as far as the N-terminus is concerned, is much lower than that of Ni(II). Anyway, Fig. S60 SI† shows that, in the presence of a 10-fold excess of Zn(II) with respect to Ni(II), the most acidic pH values are dominated by Zn(II) complexes, and, at neutral pH, about 30% of the peptide is engaged in zinc binding.

The strategy of distressing bacterial nickel homeostasis by means of competing metals (or ligands) looks promising in order to find new therapeutic ways to eradicate *H. pylori* and a detailed understanding of metal binding modes in bacterial metal chaperones is a valuable "brick in the wall" which aims to stop the pathogens from spreading.

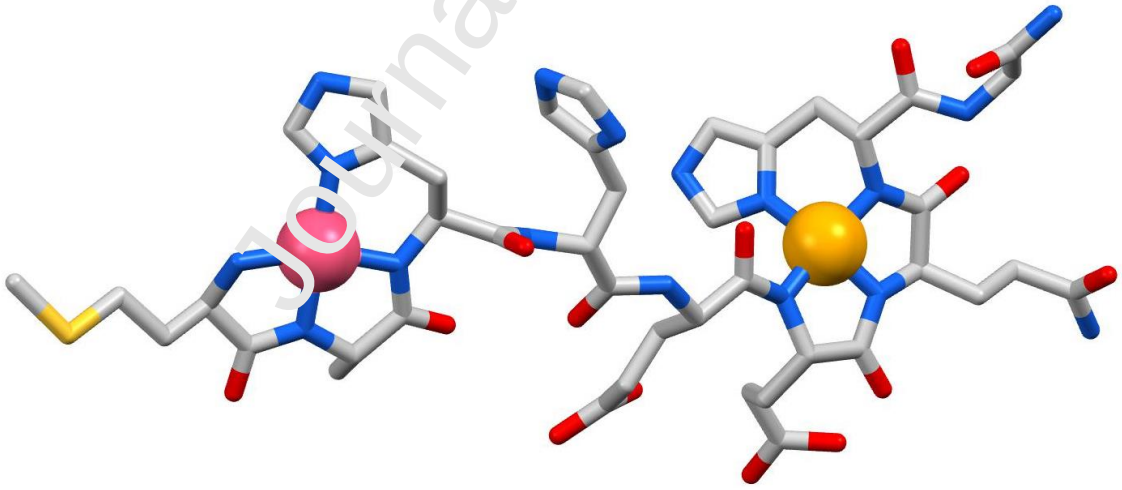

Fig. 8. Proposed molecular structure for the hetero-binuclear complex $[CuNiH_{-5}L]^{3-}$. Cu(II) atom (in purple) is bound to the ATCUN site (N_{Im}, NH_2, $2N^-$), Ni(II) atom (in yellow) displays a (N_{Im}, $3N^-$) coordination mode.

Acknowledgements

Financial support by University of Ferrara (FAR 2020), the National Science Centre (UMO-2017/26/A/ST5/00364 and 2017/26/A/ST5/00363) and by the Erasmus+ Programme are gratefully acknowledged. This paper is based upon work from COST Action CA18202, NECTAR – Network for Equilibria and Chemical Thermodynamics Advanced Research, supported by COST (European Cooperation in Science and Technology). The authors would thank dr. Claudia Stevanin for her assistance in the acquisition and interpretation of some ESI-MS spectra.

References

[1] C. de Martel, J. Ferlay, S. Franceschi, J. Vignat, F. Bray, D. Forman, M. Plummer, The Lancet Oncology, 13 (2012) 607-615.
[2] Z. Saylor, R. Maier, Microbiology, 164 (2018) 1059-1068.
[3] D.R. Scott, D. Weeks, C. Hong, S. Postius, K. Melchers, G. Sachs, Gastroenterology, 114 (1998) 58-70.
[4] N.-C. Ha, S.-T. Oh, J.Y. Sung, K.A. Cha, M.H. Lee, B.-H. Oh, Nat. Struct. Biol., 8 (2001) 505-509.
[5] J.W. Olson, R.J. Maier, Science, 298 (2002) 1788.
[6] J.V. Gilbert, J. Ramakrishna, F.W. Sunderman, A. Wright, A.G. Plaut, Infect. Immun., 63 (1995) 2682.
[7] R.J. Maier, S.L. Benoit, S. Seshadri, Biometals, 20 (2007) 655-664.
[8] S. Seshadri, S.L. Benoit, R.J. Maier, J. Bacteriol., 189 (2007) 4120-4126.
[9] G. Wang, P. Alamuri, R.J. Maier, Mol. Microbiol., 61 (2006) 847-860.
[10] H. Zeng, G. Guo, X.H. Mao, W. De Tong, Q.M. Zou, Curr. Microbiol., 57 (2008) 281-286.
[11] R. Ge, Rory M. Watt, X. Sun, Julian A. Tanner, Q.-Y. He, J.-D. Huang, H. Sun, Biochem. J., 393 (2005) 285-293.
[12] R.M. Shelake, Y. Ito, J. Masumoto, F.H. Morita, H. Hayashi, PLoS ONE, 12 (2017) e0172182-e0172182.
[13] S.V. Wegner, E. Ertem, M. Sunbul, C. He, Chem. Sci., 2 (2011) 451-456.
[14] D. Witkowska, R. Politano, M. Rowinska-Zyrek, R. Guerrini, M. Remelli, H. Kozlowski, Chem. – Eur. J., 18 (2012) 11088-11099.
[15] M. Rowinska-Zyrek, J. Zalewska-Czerwinska, A. Zawilak-Pawlik, H. Kozlowski, Dalton Trans., 43 (2014) 8976-8989.
[16] M. Rowinska-Zyrek, D. Witkowska, S. Potocki, M. Remelli, H. Kozlowski, New J. Chem., 37 (2013) 58-70.
[17] M. Rowinska-Zyrek, D. Witkowska, S. Bielinska, W. Kamysz, H. Kozlowski, Dalton Trans., 40 (2011) 5604-5610.
[18] D. Witkowska, S. Bielinska, W. Kamysz, H. Kozlowski, J. Inorg. Biochem., 105 (2011) 208-214.
[19] N.M. Chiera, M. Rowinska-Zyrek, R. Wieczorek, R. Guerrini, D. Witkowska, M. Remelli, H. Kozlowski, Metallomics, 5 (2013) 214-221.
[20] C. Harford, B. Sarkar, Acc. Chem. Res., 30 (1997) 123-130.
[21] N.L. Benoiton, Chemistry of Peptide Synthesis, Taylor & Francis, London, 2005.
[22] N.A. Sole, G. Barany, J. Org. Chem., 57 (1992) 5399-5403.
[23] P. Gans, A. Sabatini, A. Vacca, Dalton Trans., (1985) 1195-1200.
[24] P. Gans, B. O'Sullivan, Talanta, 51 (2000) 33-37.
[25] G. Gran, Acta Chem. Scand., 4 (1950) 559-577.
[26] P. Gans, A. Sabatini, A. Vacca, Talanta, 43 (1996) 1739-1753.
[27] G. Arena, R. Cali, E. Rizzarelli, S. Sammartano, Therm. Acta, 16 (1976) 315-321.
[28] C.F. Baes, M.R. S., The Hydrolysis of Cations John Wiley & Sons, Ltd, New York, 1976.
[29] L. Alderighi, P. Gans, A. Ienco, D. Peters, A. Sabatini, A. Vacca, Coord. Chem. Rev., 184 (1999) 311-318.

[30] L.D. Pettit, H.K.J. Powell, The IUPAC Stability Constants Database, Royal Society of Chemistry, London, 1992-2000.
[31] I. Sóvágó, K. Várnagy, N. Lihi, Á. Grenács, Coord. Chem. Rev., 327-328 (2016) 43-54.
[32] H. Sigel, R.B. Martin, Chem. Rev., 82 (1982) 385-426.
[33] J. Peisach, W.E. Blumberg, Arch. Biochem. Biophys., 165 (1974) 691-708.
[34] P.G. Daniele, E. Prenesti, G. Ostacoli, Dalton Trans., (1996) 3269-3275.
[35] D. Bellotti, C. Tocchio, R. Guerrini, M. Rowińska-Żyrek, M. Remelli, Metallomics, 11 (2019) 1988-1998.
[36] K. Krupa, M. Korabik, T. Kowalik-Jankowska, J. Inorg. Biochem., 201 (2019) 110819.
[37] C. Conato, H. Kozłowski, P. Młynarz, F. Pulidori, M. Remelli, Polyhedron, 21 (2002) 1469-1474.
[38] M. Rowińska-Żyrek, H. Kozłowski, Nickel Binding Sites – Coordination Modes and Thermodynamics, in: The Biological Chemistry of Nickel, The Royal Society of Chemistry, 2017, pp. 43-59.
[39] W. Bal, M. Jeżowska-Bojczuk, K.S. Kasprzak, Chem. Res. Toxicol., 10 (1997) 906-914.
[40] M. Sokolowska, A. Krezel, M. Dyba, Z. Szewczuk, W. Bal, Eur. J. Biochem., 269 (2002) 1323-1331.
[41] M. Peana, K. Zdyb, S. Medici, A. Pelucelli, G. Simula, E. Gumienna-Kontecka, M.A. Zoroddu, J. Trace Elem. Med Biol., 44 (2017) 151-160.
[42] J.D. Van Horn, G. Bulaj, D.P. Goldenberg, C.J. Burrows, J. Biol. Inorg. Chem., 8 (2003) 601-610.
[43] W. Bal, J. Lukszo, K.S. Kasprzak, Chem. Res. Toxicol., 9 (1996) 535-540.
[44] W. Bal, H. Kozlowski, R. Robbins, L.D. Pettit, Inorg. Chim. Acta, 231 (1995) 7-12.
[45] Á. Grenács, A. Kaluha, C. Kállay, V. Jószai, D. Sanna, I. Sóvágó, J. Inorg. Biochem., 128 (2013) 17-25.
[46] H. Kozlowski, M. Łuczkowski, M. Remelli, Dalton Trans., 39 (2010) 6371-6385.
[47] G. Crisponi, M. Remelli, Coord. Chem. Rev., 252 (2008) 1225-1240.
[48] F. Crea, C. De Stefano, C. Foti, D. Milea, S. Sammartano, Curr. Med. Chem., 21 (2014) 3819-3836.
[49] J.P. Laussac, B. Sarkar, J. Biol. Chem., 255 (1980) 7563-7568.
[50] J.P. Laussac, B. Sarker, Biochemistry, 23 (1984) 2832-2838.
[51] H. Irving, R.J.P. Williams, J. Chem. Soc., (1953) 3192-3210.

Declaration of interests

☒ The authors declare that they have no known competing financial interests or personal relationships that could have appeared to influence the work reported in this paper.

☐The authors declare the following financial interests/personal relationships which may be considered as potential competing interests:

Graphical Abstract

The N-terminal portion of the Hpn protein secreted by Helicobacter pylori forms stable complexes with copper(II), nickel(II) and zinc(II). Besides the ATCUN (Amino Terminal Cu(II)- and Ni(II)-binding) motif, the presence of additional histidines favours the formation of hetero-binuclear Cu(II)-Ni(II) complexes which are predominant in solutions containing both the metals.

The N-terminal domain of *Helicobacter Pylori*'s Hpn protein: the role of multiple histidine residues

Denise Bellotti,[a,b] Angelica Sinigaglia,[a] Remo Guerrini,[a] Erika Marzola,[a] Magdalena Rowińska-Żyrek,[b] Maurizio Remelli*[a]

[a] *Department of Chemical and Pharmaceutical Sciences, University of Ferrara, Via L. Borsari 46, 44121, Ferrara, Italy. E-mail: rmm@unife.it*

[b] *Faculty of Chemistry, University of Wrocław, F. Joliot-Curie 14, 50-383, Wrocław, Poland.*

Denise Bellotti, OrcID: 0000-0002-2634-0228

Maurizio Remelli, OrcID: 0000-0002-5705-3352

Remo Guerrini, OrcID: 0000-0002-7619-0918

Erika Marzola, OrcID: 0000-0002-1428-1363

Magdalena Rowińska-Żyrek, OrcID: 0000-0002-0425-1128

Abstract

Helicobacter pylori is a gram-negative bacterium with gastric localization that can cause many gastrointestinal disorders. Its survival in the host environment strictly requires an efficient regulation of its metal homeostasis, in particular of Ni(II) ions, crucial for the synthesis of some essential enzymes. Hpn is a protein of 60 amino acids, 47% of which are histidines, expressed by *H. pylori* and avid for nickel, characterized by the presence of an ATCUN (Amino Terminal Cu(II)- and Ni(II)-binding) motif and by two further histidine residues which can act as additional metal anchoring sites. We decided to deepen the following aspects: *(i)* understanding the role of each histidine in the coordination of metal ions; *(ii)* comparing the binding affinities for Cu(II), Ni(II) and Zn(II) ions, which are potentially competing metals *in vivo*; *(iii)* understanding the Hpn ability of forming ternary and poly-nuclear complexes. For these purposes, we synthesised the Hpn N-terminal "wild-type" sequence (MAHHEEQHG-Am) and the following peptide analogues: MAAHEEQHG-Am, MAHAEEQHG-Am, MAHHEEQAG-Am and MAHAEEQAG-Am. Our results highlight that the histidines in position 4 and 8 lead to the formation of Cu(II) binuclear complexes. The ATCUN motif is by far the most efficient binding site for Cu(II) and Ni(II), while macrochelate Zn(II) complexes are formed thanks to the presence of several suitable anchoring sites (His and

Glu). The metal binding affinities follow the order Zn(II) < Ni(II) << Cu(II). In solutions containing equimolar amount of wild-type ligand, Cu(II) and Ni(II), the major species above pH 5.5 are hetero-binuclear complexes.

Keywords

Copper, Nickel, Zinc, Metal complexes, Hpn protein, ATCUN motif

Introduction

Helicobacter pylori is a spiral-shaped gram-negative bacterium that can survive and proliferate in the human stomach; it is present in about half of the Earth population. *H. pylori* infection can cause serious disorders such as gastro-duodenal ulcer, MALT (mucosa-associated lymphoid tissue) lymphoma and gastric cancer, which is responsible for almost one million deaths worldwide every year [1]. The World Health Organization has classified *H. pylori* as a "Group 1" human carcinogen [2]. The survival capacity of the bacterium is especially based on the activity of urease, a nickel-containing enzyme that catalyzes the hydrolysis of urea to ammonia and bicarbonate which act as buffers and allow *H. pylori* to keep neutral the pH of its cytoplasm [3]. Urease represents about 10% of the total soluble proteins of *H. pylori* and requires up to 24 nickel ions [4]. Another enzyme that contains nickel, and also important for *H. pylori*, is the [NiFe] hydrogenase, which allows the bacterium to exploit molecular hydrogen as an alternative energy source [5].

Nickel is therefore crucial for the virulence of *H. pylori*, which contains a rather complicated management system for the homeostasis of this metal ion. This system includes a small cytoplasmic protein, called Hpn (*Helicobacter pylori* protein with affinity for nickel) [6], rich in histidine, which accounts for about 2% of the total synthesized proteins.

The role played by Hpn in *H. pylori* is not fully understood; this protein was initially considered to store nickel in the cell and to alleviate the metal toxicity by sequestering the intracellular excess of nickel [7]. In fact, it was reported that *H. pylori* mutants with Hpn deficiencies are more sensitive to excess of Ni(II) than the wild-type bacterium [8]. Interestingly, it has also been observed that, under acidic conditions, Hpn releases the bound nickel and it has been suggested that this allows the protein to supply nickel to the cell when urease activity needs to be stimulated for pH regulation [9, 10]. Recently, it has also been proposed that Hpn interacts

with many other proteins to perform various cellular functions connected with the maturation of enzymes that contain nickel, with the recovery of peptides and the acquisition of nitrogen [2].

Using equilibrium dialysis and subsequent analysis by ICP-MS and UV/visible spectrophotometry, Ge et al. have shown that Hpn binds five Ni(II) ions per monomer at pH 7.4 [11]; however, the measured dissociation constant was quite modest (K_d = 7.1·10^{-6} mol dm^{-3}). A more recent study has confirmed that Hpn can bind up to six Ni(II) ions per monomer [12]. On the other hand, an investigation carried out by converting Hpn into a FRET-based fluorescent sensor [13] reported a K_d value *in vitro* as low as 7.89·10^{-8} mol dm^{-3}, while it was not possible to measure any affinity of the Hpn-FRET (Förster resonance energy transfer) probe for Ni(II) within *E. coli*, most likely due to the severe control of the levels of this potentially toxic metal inside the cell.

MAHHEEQHGG^{10} HHHHHHHTHH^{20} HHYHGGEHHH^{30} HHHSSHHEEG^{40} CCSTSDSHHQ^{50} EEGCCHGHHE^{60}

Scheme 1. Amino acid sequence of Hpn protein. The studied N-terminal fragment is underlined; His residues are shown in green and Cys residues in red.

Hpn contains 60 amino acids, 28 of which (47%) are histidines [6]) (see Scheme 1). Hpn has several domains capable of coordinating metal cations [14-16], such as the poly-histidine sequences in the positions 11–17, 18-26 and 28–33 [14], the two motifs encompassing a double cysteine residue (EEGCC), in the positions 38–42 and 51–55 [17] and the amino-terminal sequence (Met-Ala-His-), containing a His residue in the third position, which makes it particularly suitable to bind divalent metal ions such as Cu(II) and Ni(II) [18, 19]. The coordination ability of this latter sequence, called "ATCUN" (Amino Terminal Cu(II)- and Ni(II)-binding motif) is highly recognized [20] and it has already been studied in the past by our research team, but only in conditions of ligand excess [18].

Although the first three Hpn residues play a major role in the Hpn binding ability towards Ni(II), the additional histidines in positions 4 and 8 can have a non-negligible effect on the stability of the metal complexes, for two main reasons: (i) they can take part in the formation of complexes, forming macrochelated species; (ii) they can anchor a second metal ion. We therefore decided to take a deeper look to these aspects by following two main lines of investigation. First, comparing the affinity towards the Cu(II), Ni(II) and Zn(II) ions of the model peptide corresponding to the N-terminal domain of Hpn, MAHHEEQHG-Am (wild-type, **WT**), with that of its mutants

obtained by substitution of one or two His residues with alanine (Ala-scan): MAAHEEQHG-Am (**H3A**), MAHAEEQHG-Am (**H4A**), MAHHEEQAG-Am (**H8A**) and MAHAEEQAG-Am (**H4A/H8A**) (Scheme S1, SI†). All the peptides are protected by amidation at their C-terminus to better simulate the behaviour of the entire protein. Second, in the case of the cupric ion, the complex-formation equilibria under condition of metal excess have been studied, in order to detect the formation of binuclear complexes. Stoichiometry and thermodynamic stability of the formed species have been studied by mass spectrometry and potentiometry under a wide range of pH; the structural hypotheses of the main complexes detected in solution have been suggested on the basis of the results of several spectroscopic techniques.

Experimental

Materials

$CuCl_2$, $ZnCl_2$ and $NiCl_2$ were extra pure products (Sigma-Aldrich); the concentrations of their stock solutions were standardised by EDTA titration and periodically checked *via* ICP-OES. The carbonate-free stock solutions of 0.1 mol dm^{-3} KOH were prepared by diluting concentrated KOH (Sigma-Aldrich) and then potentiometrically standardized with the primary standard potassium hydrogen phthalate (99.9% purity). All sample solutions were prepared with freshly prepared Milli-Q® water. The HCl and HNO_3 stock solutions were prepared by diluting concentrated ultra-pure HCl and HNO_3 (Sigma-Aldrich) and then standardized with KOH. The ionic strength was adjusted to 0.1 mol dm^{-3} by adding KCl (Sigma-Aldrich). Grade A glassware was employed throughout.

Peptide synthesis and purification

All the peptides were synthesized according to published methods [21] using Fmoc (fluorenylmethoxycarbonyl protecting group)/t-butyl chemistry with a Syro XP multiple peptide synthesizer (MultiSynTech GmbH, Witten Germany). Rink amide MBHA resin was used as a solid support for the synthesis of all derivatives. Fmoc-amino acids (4-fold excess) were sequentially coupled to the growing peptide chain using DIPCDI/HOBt (N,N'-diisopropylcarbodiimide/1-hydroxybenzotriazole) (4-fold excess) as activating mixture for 1h at room temperature. Cycles of deprotection of Fmoc (40% piperidine/ N,N-dimethylformamide) and coupling with the subsequent amino acids were repeated until the desired peptide-bound resin was completed. N-

terminal acetylation has been performed with acetic anhydride (0.5 mol dm^{-3}) with the presence of N-methylmorpholine (0.25 mol dm^{-3}) (3:1 v/v; 2 mL / 0.2 g of resin) as the last synthetic step. The protected peptide-resin was treated with reagent B [22] (trifluoroacetic acid (TFA) / H20 / phenol / triisopropylsilane 88 : 5 : 5: 2; v/v; 10 mL / 0.2 g of resin) for 1.5 h at room temperature. After filtration of the resin, the solvent was concentrated in vacuo and the residue triturated with ethyl ether. Crude peptides were purified by preparative reversed-phase HPLC using a Water Delta Prep 3000 system with a Jupiter column C18 (250 x 30 mm, 300 A, 15 µm spherical particle size). The column was perfused at a flow rate of 20 mL/min with a mobile phase containing solvent A (5%, v/v, acetonitrile in 0.1% TFA), and a linear gradient from 0 to 30% of solvent B (60%, v/v, acetonitrile in 0.1% TFA) over 25 min for the elution of peptides. Analytical HPLC analyses were performed on a Beckman 116 liquid chromatograph equipped with a Beckman 166 diode array detector. Analytical purity of the peptides has been assessed using a Zorbax C18 column (4.6 x 150 mm, 3 µm particle size) with the above solvent system (solvents A and B) programmed at a flow rate of 0.5 mL / min using a linear gradient from 0% to 50% B over 25 min. All analogues showed ≥ 95% purity when monitored at 220 nm. Molecular weight of final compounds was determined by a mass spectrometer ESI Micromass ZMD-2000.

Potentiometry

Stability constants for proton and metal complexes were calculated from pH-metric titration curves registered at *T*=298 K and ionic strength 0.1 mol dm^{-3} (KCl). The potentiometric apparatus consisted of an Orion EA 940 pH-meter system provided with a Metrohm 6.0234.100, glass-body, micro combination pH electrode and a dosing system Hamilton MICROLAB 500, equipped with a 0.5 ml micro burette. The thermostated glass-cell was equipped with a magnetic stirring system, a microburet delivery tube and an inlet-outlet tube for the inert gas. High purity grade nitrogen was gently blown over the test solution in order to maintain an inert atmosphere. A constant-speed magnetic stirring was applied throughout. Solutions were titrated with 0.1 mol dm^{-3} carbonate-free KOH. The electrode was daily calibrated for hydrogen ion concentration by titrating HNO_3 with alkaline solution under the same experimental conditions as above. The standard potential and the slope of the electrode couple were computed by means of SUPERQUAD [23] and Glee [24] programs. The purities and the exact concentrations of the ligand solutions were determined by the Gran method [25]. The HYPERQUAD [26] program was employed for the overall formation constant (β) calculations, referred to the following equilibrium:

$$pM + qL + rH \leftrightarrows M_pL_qH_r$$

(charges omitted; p is 0 in the case of ligand protonation; r can be negative). Step formation constants (K_{step}) and/or acid dissociation constants (K_a) are also reported. The computed standard deviations (referring to random errors only) were given by the program itself and are shown in parentheses as uncertainties on the last significant figure. Hydrolysis constants for metal ions were taken from the literature and suitably extrapolated for the experimental conditions here employed [27, 28]. The distribution and the competition diagrams were computed using the HYSS program [29]. In particular, the latter are calculated from the binary speciation models, hypothesizing a solution containing the metal and the various ligands, and admitting that all the components compete with each other to form the respective binary complexes, without mixed species formation.

Mass spectrometry

High-resolution mass spectra were obtained on a BrukerQ-FTMS spectrometer (Bruker Daltonik, Bremen, Germany), equipped with an Apollo I electrospray ionization source with an ion funnel and on a linear ion trap LTQ XL Mass Spectrometer (Thermo Scientific, Waltham, MA, USA). The mass spectrometer was operated in the positive ion mode. The instrumental parameters for BrukerQ-FTMS spectrometer were as follows: scan range m/z 100–2500, dry gas nitrogen, temperature 453 K and ion energy 5 eV. The capillary voltage was optimized to the highest signal-to-noise ratio, corresponding to 4200 V. Experimental conditions for LTQ XL Mass Spectrometer were as follows: spray voltage 4.8 kV; sheath gas 40 a.u.; capillary temperature 523 K; capillary voltage 8–25 V and tube lens 60–120 V. The samples were prepared in a 1:1 methanol-water mixture at different pH values. The samples ($[ligand]_{tot}=5\cdot10^{-4}$ mol dm^{-3}) were directly infused at a flow rate of 3 µL min^{-1}. Data were processed using the Bruker Compass DataAnalysis 3.4 program. The mass accuracy for the calibration was better than 5 ppm, enabling together with the true isotopic pattern (using SigmaFit) an unambiguous confirmation of the elemental composition of the obtained complex.

Spectroscopic measurements

The absorption spectra were recorded on a Varian Cary50 Probe spectrophotometer, in the range 350–900 nm, using a quartz cuvette with an optical path of 1 cm. Circular dichroism (CD) spectra were recorded on a Jasco J-1500 CD spectrometer in the 200–800 nm range, using a quartz cuvette with an optical path of 1 cm in the visible and near-UV range. Electron paramagnetic resonance (EPR) spectra were recorded in liquid nitrogen on a Bruker ELEXSYS E500 CW-EPR spectrometer at X-band frequency (9.5 GHz) and equipped with an ER 036TM NMR teslameter and an E41 FC frequency counter. Ethylene glycol (30%) was used as a cryoprotectant for EPR measurements. The EPR parameters were analysed by computer simulation of the experimental spectra using WIN-EPR SIMFONIA software, version 1.2 (Bruker). The concentrations of sample solutions used for spectroscopic studies were similar to those employed in the potentiometric experiment. The UV-Vis, CD and EPR spectroscopic parameters were calculated from the spectra obtained at the pH values corresponding to the maximum concentration of each particular species, based on distribution diagrams.

Results and Discussion

Ligand protonation

The five investigated peptides possess two neighbouring Glu residues containing a carboxylic side chain which can release a proton, therefore, they can be represented as H_2L. In addition to these acidic residues, the peptides contain up to three histidines and the unprotected N-terminal amine, which is the most basic group in these ligands. The protonation constants are reported in Table 1, together with the available literature values; representative distribution diagrams are shown as Supplementary Information (Figs. S1-S5).

Table 1. Overall (log *β*) and step (log *K*) protonation constants for the studied peptides at *T*=298 K and *I*=0.1 mol dm^{-3} (KCl). WT - MAHHEEQHG-Am; H3A - MAAHEEQHG-Am; H4A - MAHAEEQHG-Am; H8A - MAHHEEQAG-Am; H4A/H8A - MAHAEEQAG-Am. Values in parentheses are standard deviations on the last significant figure.

	WT				**H3A**		**H4A**		**H8A**		**H4A/H8A**	
Species	**log*β***	**log*K***	**log*β*** [a]	**log*K*** [a]	**log*β***	**log*K***	**log*β***	**log*K***	**log*β***	**log*K***	**log*β***	**log*K***
HL^-	7.79(2)	7.79	7.76	7.76	7.81(2)	7.81	7.70(3)	7.70	7.59(1)	7.59	7.59(1)	7.59
H_2L	14.75(1)	6.96	14.69	6.93	14.58(2)	6.77	14.58(3)	6.88	14.41(1)	6.82	14.16(1)	6.57

H_3L^+	21.34(2)	6.59	21.22	6.53	20.87(3)	6.29	20.80(4)	6.22	20.39(2)	5.98	18.76(2)	4.60
H_4L^{2+}	27.06(1)	5.72	27.02	5.80	25.37(2)	4.50	25.24(5)	4.44	24.70(2)	4.31	22.43(2)	3.67
H_5L^{3+}	31.20(2)	4.14	31.17	4.15	28.89(4)	3.52	28.64(3)	3.40	28.29(2)	3.59	-	-
H_6L^{4+}	34.59(2)	3.39	34.56	3.39	-	-	-	-	-	-	-	-

[a] Witkowska et al. [18]

The protonation constants measured in the present work for the wild-type peptide are almost identical to the values previously reported [18]; in the case of mutants, no literature value is available but the present results are in excellent agreement with literature data of other peptides containing the same residues with acid/base properties [30]. The substitution of one or two His residue with Ala does not affect the basicity of the terminal amine, whose log*K* value ranges in a very narrow interval (7.59 – 7.81). As for the Glu residues, the most acidic of them is characterized by a log*K* value of 3.39 – 3.59 while the second one by a log*K* value of 4.14 – 4.60; their acidity increases (and the protonation constant decreases) with the charge of the ligand which in turn depends on the number of (protonated) His residues. Finally, the log*K* value of the side imidazole groups of histidines spans in the range 5.72 – 6.96; the available data do not allow to exactly attribute a protonation value to the single His residues, in terms of *micro*-constants. The Ala-scan is unable to identify significant differences in the acidity/basicity of the three single histidines and the only observable trend is the same already reported above for Glu residues: the higher the charge of the peptide, the lower the side-imidazole protonation-constant.

Binary Cu(II) complexes

*MAHHEEQHG-Am (wild-type **WT**)*

As observed above, the N-terminal fragment of Hpn investigated here contains an ATCUN-type metal-binding site, corresponding to the first three residues MAH-, the presence of which strongly characterize the Cu(II) and Ni(II) binding behaviour of this peptide. In a previous investigation on this system [18], performed in the presence of an excess of ligand, only the ATCUN-type coordination mode ($N_{Imidazole}$, N_{NH2}, $2N_{amide}$) was detected and the formation of only mononuclear 1:1 complexes was reported. In that case, only His in position 3 was claimed to be involved in complexation. However, the presence of two additional His residues can lead to the formation of binuclear complexes also in solutions containing Cu(II) and **WT** in equimolar amount. Therefore,

we decided to revisit this system and to extend the investigation to the case of excess of metal ion and to four new mutants where one or two histidines have been replaced by alanine.

As reported in the Experimental section, the thermodynamic investigation of complex-formation equilibria has been performed by means of potentiometric titrations on solutions where the M:L stoichiometric ratio was 0.8:1 or 1.9:1. The speciation model for the system Cu(II)/**WT**, reported in Table 2, was obtained putting all the experimental data together (8 curves, 753 experimental points in the pH range 2.5-11) and a very good fitting was obtained (σ = 1.81). Of course, given the speciation model, the shape of the corresponding distribution diagram depends on the metal and ligand concentrations: Fig. 1a shows that, when Cu(II) and **WT** are present in solution at a nearly equimolar ratio, six variously protonated mononuclear 1:1 complexes are formed in the explored pH range and they engage all the copper at pH higher than 5.2. The corresponding stoichiometries and formation constants are in very good agreement with literature values. However, at acidic pH, when "free" Cu(II) ions are still available in solution, a not negligible amount of the binuclear species $[Cu_2H_{-1}L]^+$ is formed (about 12%). On the other hand, if the metal ion is in excess, practically only binuclear complexes are formed at neutral/alkaline pH (Fig. 1b).

Table 2. Cumulative complex-formation constants (β) and acid dissociation constants (K_a) of Cu(II) complexes with the peptide MAHHEEQHG-Am (**WT**), at T = 298.2 K and I = 0.1 mol dm^{-3} (KCl). Standard deviations on the last figure in parentheses.

Species	**log β**	**pK_a**	**log β** [a]	**pK_a** [a]
$[CuH_3L]^{3+}$	25.52(8)	4.03	-	-
$[CuH_2L]^{2+}$	21.49(6)	4.39	-	-
$[CuHL]^{+}$	17.10(3)	4.57	17.38	4.72
$[CuL]$	12.53(2)	6.17	12.66	5.96
$[CuH_{-1}L]^{-}$	6.36(3)	7.05	-6.70	7.09
$[CuH_{-2}L]^{2-}$	-0.69(4)	-	-0.39	-
$[Cu_2H_{-1}L]^{+}$	10.98(2)	5.52	-	-
$[Cu_2H_{-2}L]$	5.46(3)	-	-	-
$[Cu_2H_{-4}L]^{-2}$	-9.27(3)	9.04		-
$[Cu_2H_{-5}L]^{-3}$	-18.31(5)	-	-	-

[a] Witkowska et al. [18]

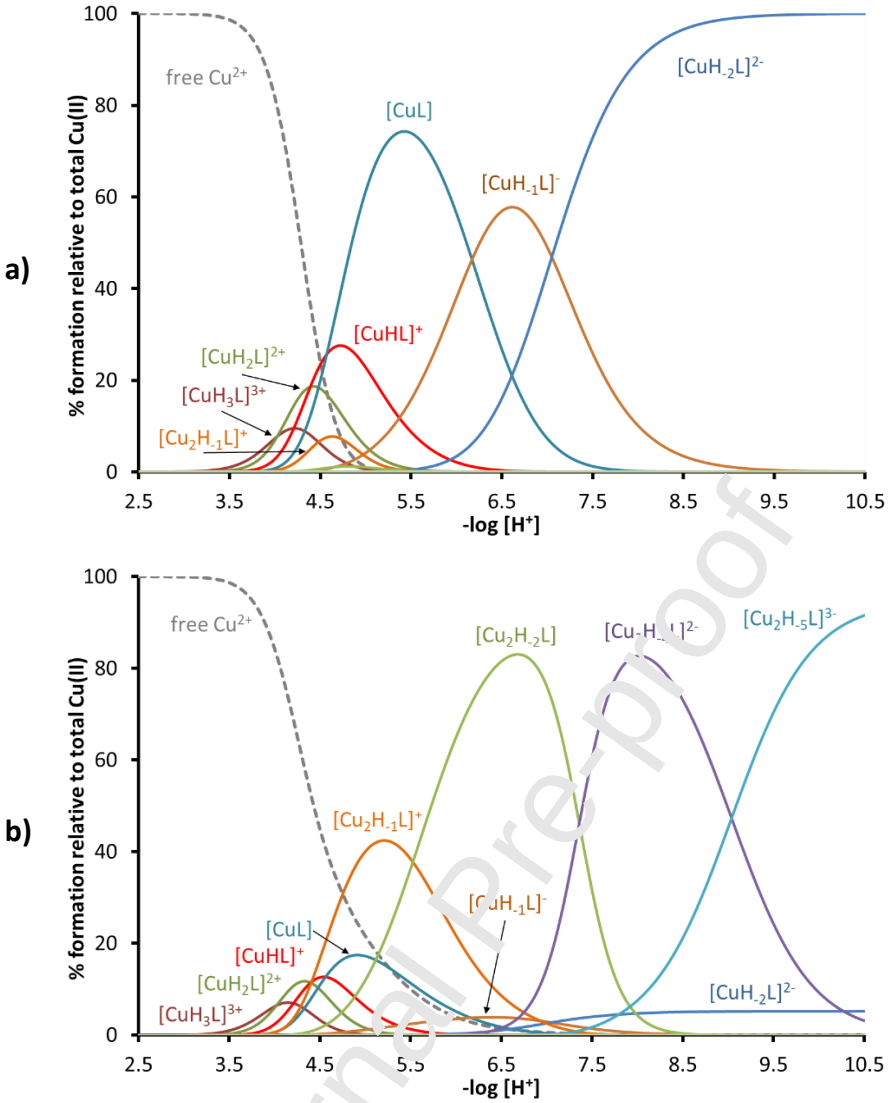

Fig. 1. Representative species distribution diagrams for complex-formation of **WT** with Cu(II), at T = 25 °C and I = 0.1 mol dm^{-3} (KCl). C_L = 1.0·10^{-3} mol dm^{-3} and a) $C_{Cu(II)}$ = 0.8·10^{-3} mol dm^{-3}; b) $C_{Cu(II)}$ = 1.9·10^{-3} mol dm^{-3}.

Starting from pH 3.5, the first detected species is $[CuH_3L]^{3+}$, whose stoichiometry indicates that only three residues involved in acid-base reactions are protonated: it is reasonable to assume that the two glutamic acids and a histidine residue are deprotonated. However, at such a pH value, histidine can be deprotonated only if it is coordinated to Cu(II) through the imidazole nitrogen of its side chain (N_{Im}); the participation of one or both carboxylate groups in chelation cannot be excluded. The species $[CuH_3L]^{3+}$ deprotonates with pK_a = 4.03 (see Table 2 and mass spectrum in Fig. S6, SI†); this value can be explained with the coordination of the terminal amine to form the species $[CuH_2L]^{2+}$, characterized by a "macrocyclic" coordination mode (N_{Im}, NH_2) [31]. By increasing the pH value, the species $[CuHL]^+$ and [CuL] begin to form, almost simultaneously, with

pK_a values of 4.39 and 4.57, respectively, compatible with the deprotonation and coordination of two amide nitrogens of the peptide chain, which occupy two further equatorial positions in the coordination sphere of the metal ion. This is the "ATCUN coordination mode": (N_{Im}, NH_2, $2N^-$). In excess of ligand (Fig. 1a), the species [CuL] reaches its formation maximum at pH 5.5 and dominates in solution in the range of pH 4.7 – 6.1, approximately. Since the formation of the first protonated species is extremely overlapped in a narrow pH range, the possibility of formation of binding isomers cannot be excluded. It is worth of note that, also in the presence of a slight excess of peptide with respect to Cu(II) (see the distribution diagram of Fig. 1a), in the acidic pH range, a not negligible amount of the binuclear $[Cu_2H_{-1}L]^+$ species is formed. Its possible structure is discussed below where the results of the investigation in excess of metal are reported.

From the qualitative Vis absorption spectra (Fig. S7, SI†) recorded at pH lower than 5.0, it is not possible to precisely identify the wavelengths of maximum absorption corresponding to the species $[CuH_3L]^{3+}$ $[CuH_2L]^{2+}$ and $[CuHL]^+$, due to the superimposition of these complexes and the interference of the exa-aquo Cu(II) ion, present in solution in a consistent amount up to pH 4.5. In the case of nearly equimolar Cu(II)/**WT** solutions, the UV-Vis spectra recorded at pH 5.0 and 5.5 are instead characterized by a single intense absorption band located at 525 nm (Fig. S7a and Table S1, SI†), almost entirely attributable to [CuL] and compatible with the coordination hypothesis (N_{Im}, NH_2, $2N^-$) suggested above (expected λ_{max} = 531 nm [32]). EPR data at pH 5.5 (Table S1, SI†) agree with a 4N coordination around Cu(II) in the equatorial plane of the complex [33]. Above pH 4.5, CD spectra (Fig. S8a and Table S1, SI†) contain two intense negative bands and one positive signal in the UV region, at 236, 272 and 311 nm, attributable to charge-transfer transitions to Cu(II) by the coordinated amine, imidazole and peptide nitrogens, respectively [34]. As for the Vis range of CD spectra, the typical double band characteristic of the ATCUN-type coordination [20] was observed. No clue was detected of a possible direct involvement of methionine sulphur in peptide coordination.

Finally, again in the presence of ligand excess (Fig. 1a), at neutral/alkaline pH, the species $[CuH_{-1}L]^-$ and $[CuH_{-2}L]^{2-}$ are formed, through two deprotonation steps involving the remaining two histidine residues, which do not participate in the complex formation. In fact, the corresponding pK_a values are respectively 6.17 and 7.05 (Table 2), rather close to those obtained for the free ligand (6.59 and 6.96) (Table 1). This hypothesis is also confirmed by all the spectroscopic data which do not change by increasing the pH value from 5 to 10, as expected if the coordination mode does not change.

The system Cu(II)/**WT** has been explored also at the metal/ligand ratio of $(1.9:1)\cdot10^{-3}$ mol dm^{-3}. As expected, this favours the formation of binuclear species (see ESI-MS spectrum of Fig. S9, ESI†) where two Cu(II) ions are coordinated to the same peptide molecule (Fig. 1b). Under these experimental conditions, the complex $[Cu_2H_{-1}L]^+$, which is formed starting from pH 4, reaches a percentage of about 45%, being the predominant species around pH 5.5. It is reasonable to assume that, while one Cu(II) ion is coordinated to the N-terminal domain in the above described ATCUN mode, the second metal atom is bound to one of the two remaining histidines of the chain, with the possible participation of one or both the side carboxylate groups of Glu residues; the stoichiometry of this complex requires that the third histidine is still protonated. Available data do not allow to state if the "anchor" of the second Cu(II) ion is His-4 or His-8; a mixture of these two species is likely. In the pH range 5–8, the third histidine releases its proton, leading to the species $[Cu_2H_{-2}L]$, which dominates at pH 6–7. The corresponding pK_a value (5.52, Table 2) much lower than that measured in the absence of copper (6.96, Table 1), suggests that this His binds the second Cu(II) ion. Moving to alkaline pH, the species $[Cu_2H_{-4}L]^{2-}$ is formed: two protons are released in a quick sequence, probably corresponding to the deprotonation and coordination of two peptide nitrogens. A further deprotonation step is observed at the most alkaline pH values, characterized by a pK_a value of 9.04; it can be attributed to the coordination of a third amide nitrogen, which most likely substitutes one imidazole in the equatorial plane of the complex, leading to the formation of the species $[Cu_2H_{-5}L]^{3-}$, whose binding mode is $(N_{Im}, NH_2, 2N^-)(N_{Im}, 3N^-)$. In principle, both His-4 and His-8 can originate this binding mode, where the peptide wraps around the second Cu(II) ion through the coordination of the amide nitrogens of its peptide chain. The significant difference is that, if His-4 is bound to copper in the equatorial plane of the complex, the amide coordination should proceed in the C-terminal direction (due to the presence of the other complexed metal ion) while, in the case of His-8, it can proceed towards the N-terminus. It is well known in the literature that both these modes are possible, but the latter leads to more stable complexes than the former due to the different dimension of the formed chelation rings [35, 36].

Spectroscopic data (Figs. S7b and S8b; Table S2, SI†) confirm the above hypotheses. The two Vis absorption spectra recorded at pH 4.5 and 5.0, where the complex $[Cu_2H_{-1}L]^+$ is the prevailing species in solution, show two maxima: the first, more intense, at λ_{max} = 528 nm corresponds to the ATCUN coordination mode of the first Cu(II) ion. The second band, around λ_{max} = 740-730 nm, can be attributed to the coordination of an imidazole nitrogen to the second copper atom with the possible participation of the side carboxylate group of one Glu residue (expected absorption

maximum: 731 nm [32]). Increasing the pH, the second band shifts to shorter wavelengths, as a consequence of the coordination of further nitrogens to the second Cu(II) in the C-terminal domain of **WT**. At pH = 11, only one intense absorption band is observed at 520 nm, typical of a Cu(II) species where 3 amidic nitrogens of the peptide chain and one imidazole are bound to the equatorial plane of the complex (expected λ_{max} = 522 nm [32]). This is exactly the coordination mode suggested above for the second metal ion in the complex $[Cu_2H_{-5}L]^{3-}$. This band is superimposed to that of the ATCUN-type copper. EPR spectra recorded in the presence of excess of Cu(II) are very weak, confirming the formation of binuclear complexes. CD spectra (Fig. S8b and Table S2, SI†) at pH 5 are practically identical to those already described above for the solutions containing an excess of ligand and referring to the ATCUN-type complex. However, when the Cu(II) ion is instead in excess, increasing the pH value, the shape of CD spectra undergoes a dramatic change, due to the contribution of the second Cu(II) ion. The final spectrum, at pH 10.2, is very similar to that already previously reported for a Cu(II)/peptide binding mode (N_{Im}, $3N^-$) [37], attributable to the species $[Cu_2H_{-5}L]^{3-}$.

*MAAHEEQHG-Am (**H3A**)*

The thermodynamic complex-formation constants for the system Cu(II)/**H3A** are reported in Table 3 and the corresponding distribution diagrams are shown in Fig. 2.

Table 3. Cumulative complex-formation constants (β) and acid dissociation constants (K_a) of Cu(II) complexes with the peptide MAAHEEQHG-Am (**H3A)**, at T = 298.2 K and I = 0.1 mol dm^{-3} (KCl). Standard deviations on the last figure in parentheses.

Species	**log β**	**pK_a**
$[CuH_2L]^{2+}$	19.59(3)	4.93
$[CuHL]^{+}$	14.66(2)	5.62
[CuL]	9.04(3)	6.82
$[CuH_{-1}L]^{-}$	2.22(4)	7.30
$[CuH_{-2}L]^{2-}$	-5.08(5)	10.14
$[CuH_{-3}L]^{3-}$	-15.22(7)	-
$[Cu_2H_{-1}L]^{+}$	6.76(4)	-
$[Cu_2H_{-3}L]^{-}$	-6.53(4)	7.68
$[Cu_2H_{-4}L]^{-2}$	-14.21(6)	9.03
$[Cu_2H_{-5}L]^{-3}$	-23.24(7)	11.0
$[Cu_2H_{-6}L]^{-4}$	-34.2(1)	-

The **H3A** peptide is the only one, in the series here investigated, that does not have a histidine in third position: this definitively influences its ability to coordinate the Cu(II) ion, resulting in complexes which are significantly weaker than those formed by **WT** (over 3.5 orders of magnitude in the case of the species [CuL]). However, the presence of two histidines, separated by three amino acid residues, allows, also in this case, the formation of binuclear complexes, as demonstrated by the mass spectrum of Fig. S10b SI†, recorded in excess of metal.

The first species observed at acidic pH is the complex $[CuH_2L]^{2+}$, the main complex up to pH 5. Both its stoichiometry and the spectroscopic parameters (Figs. S11 and S12, Table S3, SI†) suggest that the metal is bound to the nitrogen of a histidine imidazole side chain, with the possible participation of the carboxylic group of a glutamic acid. Since the sequence contains two His and two Glu residues, it is likely a mixture of complexes in solution with this type of coordination but with different donor atoms involved. The loss of a proton leads to the formation of the $[CuHL]^{+}$ complex, which reaches its maximum at pH 5.5; the experimental value of λ_{max} is very close to that expected for a coordination ($2N_{Im}$, COO^-), with the formation of a macrochelate between the two histidines. The corresponding pK_a value (4.98), considerably lower than that measured for the second histidine in the absence of metal (6.77, Table 1), supports this coordination hypothesis.

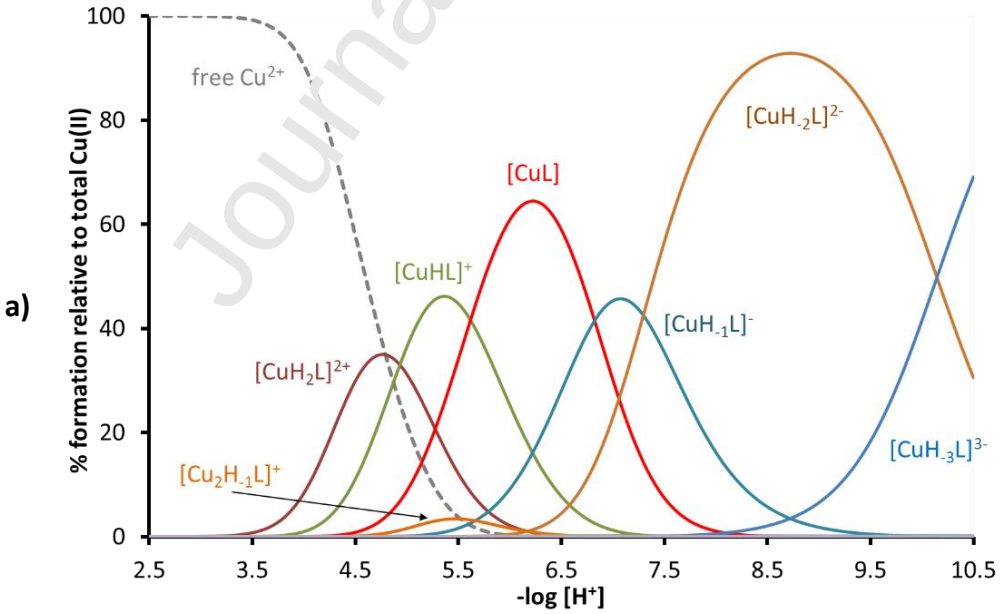

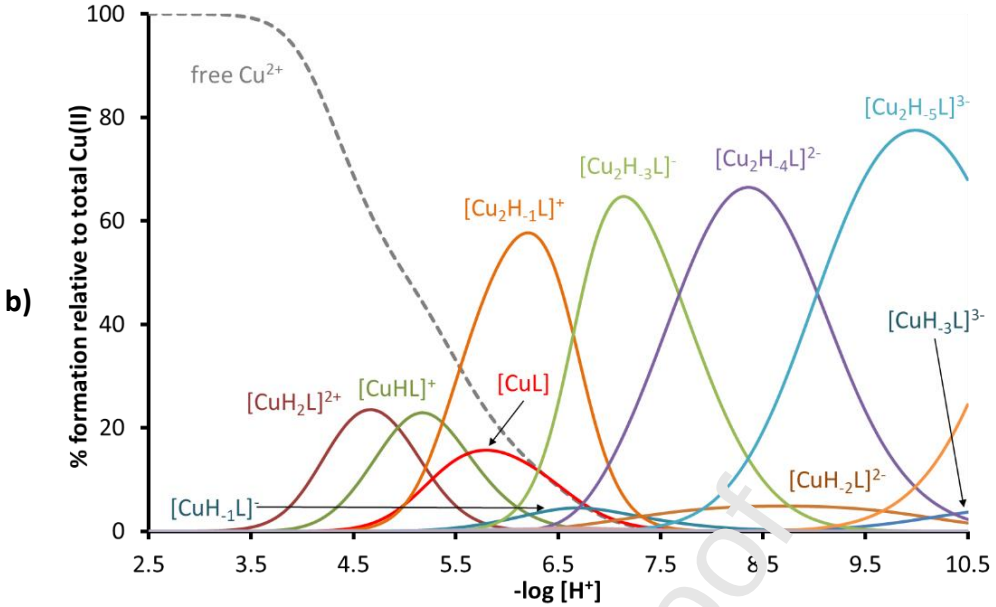

Fig. 2. Representative species distribution diagrams for complex-formation of **H3A** with Cu(II), at *T* = 25 °C and *I* = 0.1 mol dm^{-3} (KCl). $C_L = 1.0 \cdot 10^{-3}$ mol dm^{-3} and a) $C_{Cu(II)} = 0.8 \cdot 10^{-3}$ mol dm^{-3}; b) $C_{Cu(II)} = 1.9 \cdot 10^{-3}$ mol dm^{-3}.

Starting from pH 4.5, the formation of the complex [CuL] is observed (Fig. 2a). The thermodynamic and spectroscopic parameters suggest the deprotonation and coordination of the terminal amino group, which replaces an imidazole ring in the equatorial plane of the complex (N_{Im}, NH_2, COO^-); the fourth vertex of the plane is probably occupied by a water molecule, while the second imidazole ring becomes free or interacts with the metal in axial position. When, on the other hand, the metal ion is in excess, the binuclear complex $[Cu_2H_{-1}L]^+$ forms in a considerable amount, in parallel with [CuL]. Here, the additional metal ion is linked to the second histidine and to an amide nitrogen of the peptide chain. Both the complex [CuL] and the species $[Cu_2H_{-1}L]^+$, have their formation maximum around pH 6. As pH increases, each metal ion anchored to the peptide is able to gradually displace the amide protons of the chain, thus binding the corresponding amide nitrogens. The wavelength of maximum absorption in the Vis spectra shifts to lower values as the pH increases: the absorption band is narrower and more intense when only mononuclear complexes are present (with a unique and well-defined coordination site) while it is broader for binuclear complexes that contain two similar but not identical metal-binding sites. The CD spectra (Fig. S12, SI†) have very similar shapes, especially in their UV portion, confirming that the type of donor atoms is the same in the two cases.

*MAHAEEQHG-Am (**H4A**)*

The thermodynamic complex-formation constants for the system Cu(II)/**H4A** are reported in Table 4 and the corresponding distribution diagrams are shown in Fig. 3.

Table 4. Cumulative complex-formation constants (β) and acid dissociation constants (K_a) of Cu(II) complexes with the peptide MAHAEEQHG-Am (**H4A)**, at T = 298.2 K and I = 0.1 mol dm^{-3} (KCl). Standard deviations on the last figure in parentheses.

Species	**log β**	**pK_a**
$[CuHL]^{+}$	15.15(3)	4.60
[CuL]	10.55(3)	4.71
$[CuH_{-1}L]^{-}$	5.84(2)	6.83
$[CuH_{-2}L]^{2-}$	-0.99(4)	-
$[Cu_2H_{-1}L]^{+}$	8.74(5)	5.76
$[Cu_2H_{-2}L]$	2.98(7)	6.56
$[Cu_2H_{-3}L]^{-}$	-3.58(7)	6.34
$[Cu_2H_{-4}L]^{-2}$	-9.92(3)	8.88
$[Cu_2H_{-5}L]^{-3}$	-18.80(4)	-

The replacement of histidine in position 4 with an alanine does not preclude the peptide **H4A** from complexing Cu(II) as described above for **WT**: in fact, His in third position leads to the formation of the stable ATCUN-type complexes, while the presence of a second histidine in position 8 allows the formation of binuclear complexes. The presence of the latter species, detected by potentiometry, was confirmed by the mass spectra recorded in excess of metal (Fig. S13, SI†). The speciation model of Table 4 does not differ very much from that determined for the **WT** peptide (Table 2) except for the absence of the most protonated species $[CuH_3L]^{3+}$ and $[CuH_2L]^{2+}$; this is obviously due to the lack of one histidine residue. In excess of ligand, the ATCUN-type complex, with stoichiometry $[CuH_{-1}L]^{-}$, is already the predominant species at pH 5; at alkaline pH, the second histidine releases the proton bound to the pyridine-type nitrogen of its imidazole ring, with a pK_a value (6.83) very similar to that measured in the absence of metal (6.88), thus suggesting the absence of any interaction with the Cu(II) ion already bound to the N-terminal domain. The Vis-absorption (Fig. S14a, SI†) and the CD spectra (Fig. S15a, SI†) confirm this coordination hypothesis, since they are practically unchanged throughout the explored pH range (Table S5, SI†). Interestingly, although the replacement of His in position 4 with Ala does not

change the peptide coordination modes, the mono-nuclear complexes of **WT** are more stable than those formed by **H4A** (see competition diagrams discussed below). This result is in agreement with the observation, already widely documented in the literature, that the number of histidine residues of the peptide sequence always has a great influence on the stability of the formed Cu(II) complexes, due to the possibility of forming a number of species with the same stoichiometry but a different set of donor atoms. Lastly, in the presence of metal excess, the spectroscopic data (Figs. S14b and S15b, Table S6, SI†) have a very similar trend to that already discussed above for **WT**, confirming the formation of binuclear species with similar structure and stability of those already described for **WT**.

a)

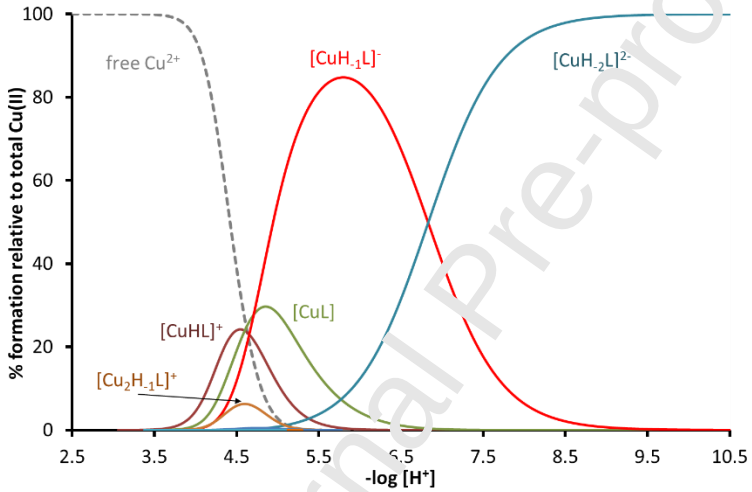

b)

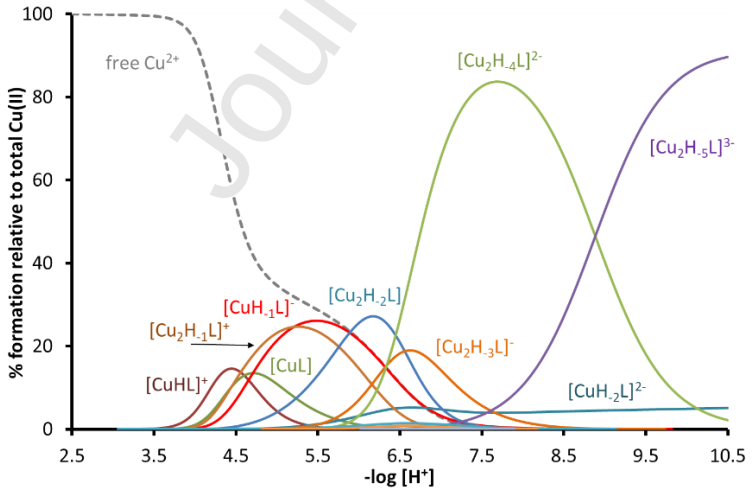

Fig. 3. Representative species distribution diagrams for complex-formation of **H4A** with Cu(II), at T = 25 °C and I = 0.1 mol dm^{-3} (KCl). C_L = 1.0·10^{-3} mol dm^{-3} and a) $C_{Cu(II)}$ = 0.8·10^{-3} mol dm^{-3}; b) $C_{Cu(II)}$ = 1.9·10^{-3} mol dm^{-3}.

*MAHHEEQAG-Am (**H8A**)*

The thermodynamic complex-formation constants for the system Cu(II)/**H8A** are reported in Table 5 and the corresponding distribution diagrams are shown in Fig. 4.

Table 5. Cumulative complex-formation constants (β) and acid dissociation constants (K_a) of Cu(II) complexes with the peptide MAHHEEQAG-Am (**H8A)**, at T = 298.2 K and I = 0.1 mol dm^{-3} (KCl). Standard deviations on the last figure in parentheses.

Species	**log β**	**pK_a**
$[CuH_2L]^{2+}$	19.33(2)	-
[CuL]	10.55(1)	4.87
$[CuH_{-1}L]^{-}$	5.68(2)	6.76
$[CuH_{-2}L]^{2-}$	-1.08(4)	-
$[Cu_2H_{-1}L]^{+}$	8.82(5)	5.82
$[Cu_2H_{-2}L]$	3.00(7)	-
$[Cu_2H_{-4}L]^{-2}$	13.12(3)	9.32
$[Cu_2H_{-5}L]^{-3}$	-22.44(4)	-

The **H8A** peptide contains two histidine residues which, although close together, can lead to the formation of binuclear species. A first metal ion is bound by the N-terminal ATCUN site, starting from pH 3, and this complex (variously protonated depending on pH) is practically the only species in solution in the presence of ligand excess. If, on the other hand, the metal is in excess, a second Cu(II) ion can first anchor to the histidine in position 4 and then bind, at basic pH, the amides of the peptide backbone in the C-terminal direction. The formation of binuclear complexes, suggested by the potentiometric results of Table 5, is confirmed by the mass spectra, an example of which is shown in Fig. S16 SI†). The spectrophotometric results confirm a behaviour similar to that of the other peptides (Figs. S17 and S18, Tables S7 and S8, SI†). It is worth of note that two consecutive histidines really do give rise to binuclear complexes.

a)

b)

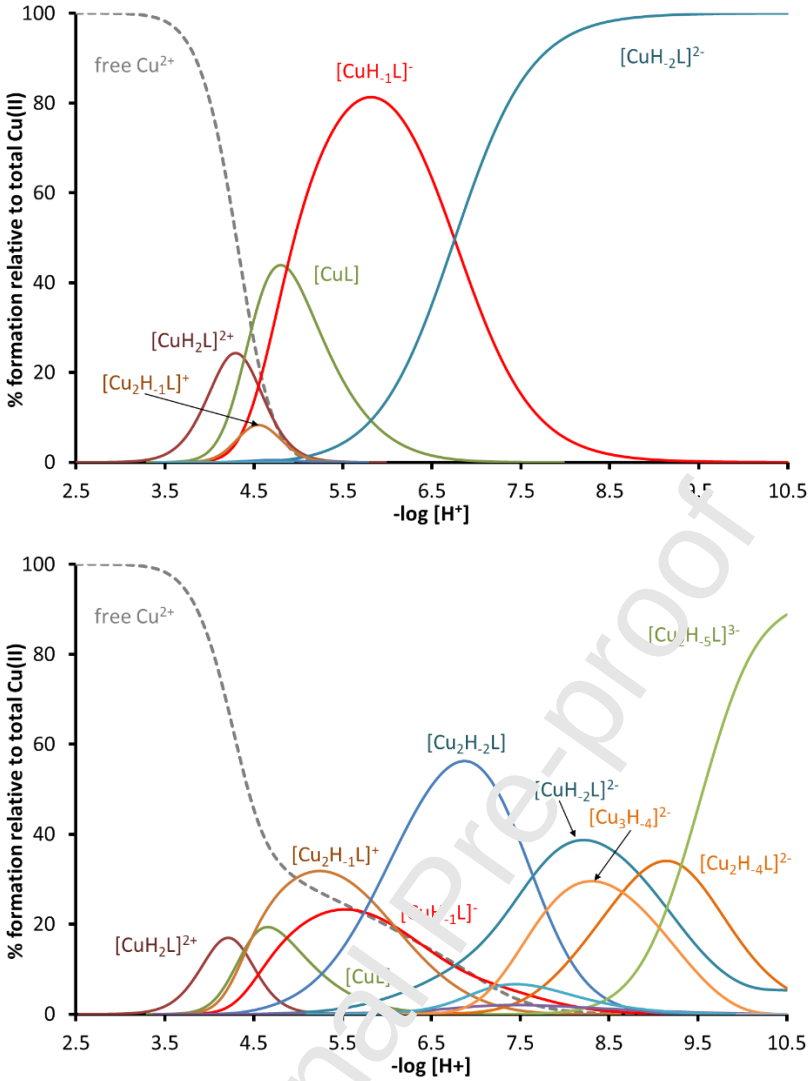

Fig. 4. Representative species distribution diagrams for complex-formation of **H8A** with Cu(II), at T = 25 °C and I = 0.1 mol dm^{-3} (KCl). C_L = 1.0·10^{-3} mol dm^{-3} and a) $C_{Cu(II)}$ = 0.8·10^{-3} mol dm^{-3}; b) $C_{Cu(II)}$ = 1.9·10^{-3} mol dm^{-3}.

*MAHAEEQAG-Am (**H4A/H8A**)*

Table 6. Cumulative complex-formation constants (β) and acid dissociation constants (K_a) of Cu(II) complexes with the peptide MAHAEEQAG-Am (**H4A/H8A)**, at T = 298.2 K and I = 0.1 mol dm^{-3} (KCl). Standard deviations on the last figure in parentheses.

Species	**log β**	**pK_a**
$[CuHL]^{+}$	12.95(1)	-
$[CuH_{-1}L]^{-}$	4.27(1)	5.28
$[CuH_{-2}L]^{2-}$	-0.99(1)	-

The thermodynamic complex-formation constants for the system Cu(II)/MAHAEEQAG-Am (**H4A/H8A**), are reported in Table 6 and the corresponding distribution diagram is shown in Fig. 5.

Only the histidine in third position is present in this peptide and, therefore, only mononuclear, ATCUN-type complexes are formed in the explored pH range. In addition, Vis absorption data (Fig. S19, Table S9, SI†) show that, in the presence of Cu(II) excess, the solution becomes cloudy at pH > 7 for the formation of a precipitate, most likely of Cu(II) hydroxide. CD spectra (Fig. S20, Table S9, SI†) are almost identical at 0.8:1.0 and 1.9:1.0 metal-to-ligand ratios, supporting the absence of polynuclear complexes.

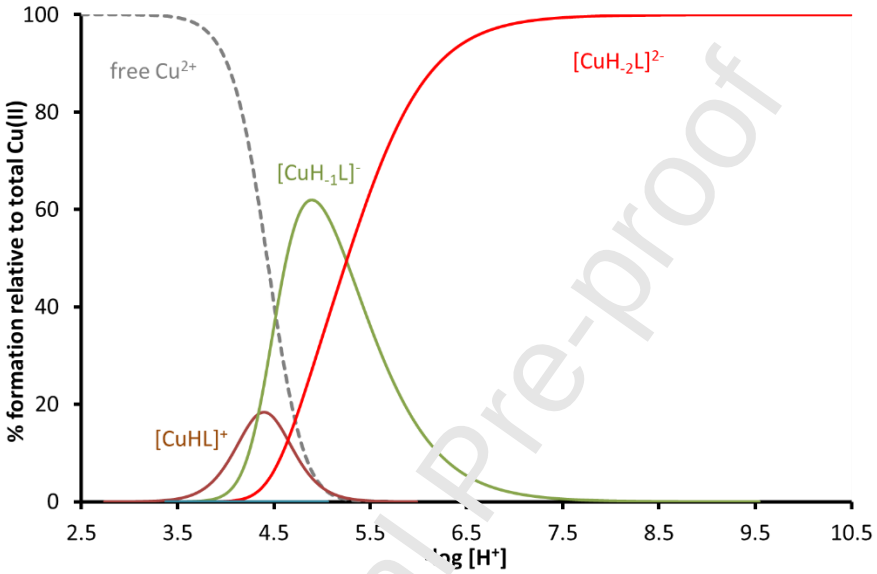

Fig. 5. Representative species distribution diagram for complex-formation of **H4A/H8A** with Cu(II), at T = 25 °C and I = 0.1 mol dm^{-3} (KCl). C_L = 1.0·10^{-3} mol dm^{-3} and $C_{Cu(II)}$ = 0.8·10^{-3} mol dm^{-3}.

Binary Ni(II) complexes

The complex-formation equilibria with the Ni(II) ion have been investigated only in the presence of ligand excess and only mono-nuclear complexes have been detected. The speciation models obtained by potentiometry are shown in Table 7, while the corresponding distribution diagrams and all the spectroscopic results are reported as SI† (Figs. S22-S41, Tables S10–S14). The formation of yellow, diamagnetic, square-planar complexes has been observed at alkaline pH in every system, with a slow kinetics which required rather long waiting times between each titrant addition. No precipitation was observed in the explored pH range.

The presence of the ATCUN type sequence in all peptides, with the exception of **H3A**, favours the Ni(II) coordination to the amino-terminal domain, as already described for copper. The

main species at neutral pH is the (N_{Im}, NH_2, $2N^-$) complex, characterized by an intense absorption around 422 nm [20, 38]; the corresponding CD spectrum contains, in the Vis range, two bands of opposite sign, at 415 (positive) and 480 (negative) nm, respectively [39-41], and a positive and intense charge-transfer band in the UV region around 260 nm [42, 43]. However, it should be noted that the shape of CD spectra referring to the peptides **WT** and **H4A** progressively changes at pH>9, although no variations are observed either in the absorption spectra or in the distribution diagrams (where the complex $[NiH_{-2}L]^{2-}$ is practically the only species detected in solution at pH> 8). On the contrary, for the **H8A** and **H4A/H8A** peptides, in which the histidine in position 8 has been replaced by an alanine, the CD spectrum simply becomes more intense, as pH increases, without changing shape. Evidently, His-8, when present, is somehow involved in coordination at high pH, for example with a shift of nickel from the N-terminal to the C-terminal domain. However, the available experimental data are not enough to fully clarify this point, which would require further investigation.

A peculiar behaviour is that of **H3A**, due to the lack of the ATCUN-type coordination domain. Likely, at acidic pH, the Ni(II) ion is anchored to one His residue [38, 44] and then, as pH increases, macrochelated species are formed, with the involvement of the second histidine and/or of the terminal amino group. The species formed at acidic pH are probably octahedral; they evolve to the classical square planar, low spin complex at alkaline pH, with the involvement of deprotonated amide nitrogens of the backbone. As a matter of fact, up to four deprotonation steps are revealed by potentiometry at alkaline pH, suggesting the coordination of more than two amide nitrogens to Ni(II). This behaviour is confirmed by spectroscopic data (Figs. S28 and S29, SI†): the wavelength of maximum absorption at pH > 10 is 414 nm, lower than that recorded for the other systems (about 422 nm). In addition, the CD spectra in the Vis range show a single broad and intense negative band, located around 440 nm.

Table 7. Cumulative complex-formation constants (β) and acid dissociation constants (K_a) of Ni(II) complexes with the investigated peptides, at T = 298.2 K and I = 0.1 mol dm^{-3} (KCl). Standard deviations on the last figure in parentheses.

Ligand	Species	log β	pK_a
MAHHEEQHG-Am (wild-type, **WT**)	$[NiHL]^+$	12.90(8)	5.77
	[NiL]	7.13(6)	6.26
	$[NiH_{-1}L]^-$	0.87(5)	6.95
	$[NiH_{-2}L]^{2-}$	-6.08(5)	-

MAAHEEQHG-Am (**H3A**)	$[NiH_2L]^{2+}$	18.0(2)	6.0
	$[NiHL]^{+}$	11.98(8)	6.25
	[NiL]	5.73(6)	7.78
	$[NiH_{-1}L]^{-}$	-2.05(8)	-
	$[NiH_{-3}L]^{3-}$	-18.64(7)	9.1
	$[NiH_{-4}L]^{4-}$	-27.7(1)	-
MAHAEEQHG-Am (**H4A**)	[NiL]	6.25(8)	5.49
	$[NiH_{-1}L]^{-}$	0.76(2)	6.89
	$[NiH_{-2}L]^{2-}$	-6.13(5)	-
MAHHEEQAG-Am (**H8A**)	[NiL]	6.01(6)	5.75
	$[NiH_{-1}L]^{-}$	0.26(3)	6.72
	$[NiH_{-2}L]^{2-}$	-6.46(4)	-
MAHAEEQAG-Am (**H4A/H8A**)	$[NiH_{-1}L]^{-}$	-0.48(5)	5.55
	$[NiH_{-2}L]^{2-}$	-6.03(1)	-

Binary Zn(II) complexes

The Zn(II) ion has a strong affinity for the imidazole nitrogen of histidine, while it is generally accepted that it is not able to displace the protons of the amide nitrogens. In all the studied systems, the formation of 1:1 complexes, variously protonated, was observed (see Table 8, distribution diagrams of Figs. S42–S46 SI† and mass spectra of Figs. S47–S51 SI†). The first complexes are formed in all systems starting from pH 4.5 – 5.5: the stoichiometry of these species depends on the number of histidines in the sequence ($[ZnH_2L]^{2+}$ in the case of **WT**; $[ZnHL]^{+}$ in the case of **H3A**, **H4A** and **H8A**; [ZnL] in the case of **H4A/H8A**). In every case, the stoichiometry requires that two nitrogen atoms are unprotonated and bound to the metal. They should belong to the two available imidazole side chains; or, in the case of **H4A/H8A**, to the histidine and the terminal amino group. It should be noted that, in the case of **WT**, which contains three histidines, a mixture of complexes, with identical stoichiometry and coordination mode but involving different donor atoms, can be formed. This may explain why the $[ZnH_2L]^{2+}$ complex of **WT** begins to form at a pH value (4.5) lower than that observed with the other peptides. It is also worth noting that, when the histidine in position 8 is replaced by an alanine (peptides **H8A** and **H4A/H8A**) the first complexes are formed only at pH around 5.5, suggesting an important role of

His-8 as the first metal anchor. All these complexes should be macrochelated, most likely with a tetrahedral geometry, where the two coordination positions not occupied by nitrogens are occupied by water molecules. As the pH increases, the third nitrogen of the peptide, if present, binds the metal by displacing a water molecule. Only in the case of **WT**, zinc can simultaneously coordinate three histidine residues. In addition, also the formation of a species with four nitrogen atoms linked to zinc is theoretically possible for **WT,** corresponding to the complex [ZnL]; this could be the reason for its greater stability (almost two orders of magnitude) compared to the other complexes of the same stoichiometry formed by the other peptides (see Table 8). Unexpectedly, the solutions containing Zn(II) and **WT** are the only ones in which the formation of a precipitate was observed between pH 7 and 10.2. In all other cases, no clouding of the solution was detected, although the potentiometric signal had a slow drift at pH> 8.5. At alkaline pH, further deprotonation steps have been observed, which lead to the formation of the species $[ZnH_{-1}L]^-$ and, only in the case of **H4A/H8A**, also $[ZnH_{-2}L]^{2-}$. The simplest explanation is the deprotonation of the coordinated water molecules.

Table 8. Cumulative complex-formation constants (β) and acid dissociation constants (K_a) of Zn(II) complexes with the investigated peptides, at T = 298.2 K and I = 0.1 mol dm^{-3} (KCl). Standard deviations on the last figure in parentheses.

Ligand	Species	log β	pK_a
MAHHEEQHG-Am (wild-type, **WT**)	$[ZnH_2L]^{2+}$	18.79(6)	6.23
	$[ZnHL]^{+}$	12.56(6)	6.46
	[ZnL]	6.10(4)	-
MAAHEEQHG-Am (**H3A**)	$[ZnHL]^{+}$	11.71(4)	6.93
	[ZnL]	4.78(4)	8.02
	$[ZnH_{-1}L]^{-}$	-3.24(5)	-
MAHAEEQHG-Am (**H4A**)	$[ZnHL]^{+}$	11.69(3)	7.22
	[ZnL]	4.47(6)	8.37
	$[ZnH_{-1}L]^{-}$	-3.9(1)	-
MAHHEEQAG-Am (**H8A**)	$[ZnHL]^{+}$	10.71(6)	6.58
	[ZnL]	4.13(3)	8.23
	$[ZnH_{-1}L]^{-}$	-4.10(4)	-
MAHAEEQAG-Am (**H4A/H8A**)	[ZnL]	3.88(6)	7.84
	$[ZnH_{-1}L]^{-}$	-3.96(6)	8.46

$[ZnH_{-2}L]^{2-}$	-12.42(6)	-

Ternary Cu(II)/Ni(II)/WT complexes

Data reported above show that, in the presence of Cu(II) excess, the **WT** peptide can form binuclear species. Therefore, we decided to test its behavior in the presence of equimolar quantities of Cu(II) and Ni(II). First, from a qualitative point of view, it was possible to observe, during the titrations with KOH, that the solution, initially colorless, assumed a pink color at acidic pH close to neutrality and then turned to orange at basic pH.

Potentiometric data processing revealed the formation of three hetero-metallic binuclear species, as reported in Table 9; the corresponding distribution diagram is shown in Fig. 6. This result is in excellent agreement with a recent study carried out under similar conditions on the AAHAAAHG octapeptide [45]. Although that paper does not report the complex-formation constants of the mixed species, the stoichiometry of the ternary complex formed at basic pH, obtained from mass spectra, is exactly $[CuNiH_{-5}L]^{3-}$, which corresponds (except for the different charge due to the different number of carboxylic groups of the sequence) to that obtained in the present investigation. Furthermore, the absorption spectra shown in Fig. 7 are very similar to those reported by Grenacs et al. [45] suggesting the same coordination geometry. Therefore, it can be assumed that, at acidic pH, Cu(II) coordinates at the N-terminus of **WT** (with the ATCUN-type coordination mode); as pH is increased, a nickel ion initially binds the two histidine residues not involved in copper coordination. Starting from pH about 9, the Ni(II) ion displaces up to 3 amide hydrogens of the peptide chain, thus forming the classic planar and diamagnetic 4N complex. It is reasonable to assume that, in the species $[CuNiH_{-5}L]^{3-}$ (which dominates at pH> 9, see Fig. 6) the Ni(II) ion is bound to His-8 and to the three preceding amides, in the N-terminal direction. In the pH range 4-5 – 8.5, the absorption spectra are practically identical and dominated by the d-d transition of the Cu(II) ATCUN-type complex; at more alkaline pH values, the typical band of the diamagnetic Ni(II) complex becomes instead evident.

ESI-MS spectra recorded at pH 5.5, 7.8 and 10.2 (Fig. S52 SI†) also highlight the formation of binuclear complexes with Cu(II) and Ni(II) at different protonation states and they are in good agreement with the speciation model obtained by potentiometry. Following the distribution diagram plotted in Figure 6, the observed more intense m/z signals correspond to the major species in solution under the given pH.

Table 9. Cumulative complex-formation constants (β) and acid dissociation constants (K_a) of mixed Cu(II)/Ni(II) complexes with peptide **WT**, at T = 298.2 K and I = 0.1 mol dm^{-3} (KCl). Standard deviations on the last figure in parentheses.

Species	**log β**	**pK_a**
$[CuNiH_{-1}L]^{+}$	9.97(6)	6.57
$[CuNiH_{-2}L]$	3.40(4)	-
$[CuNiH_{-5}L]^{3-}$	-23.74(4)	-

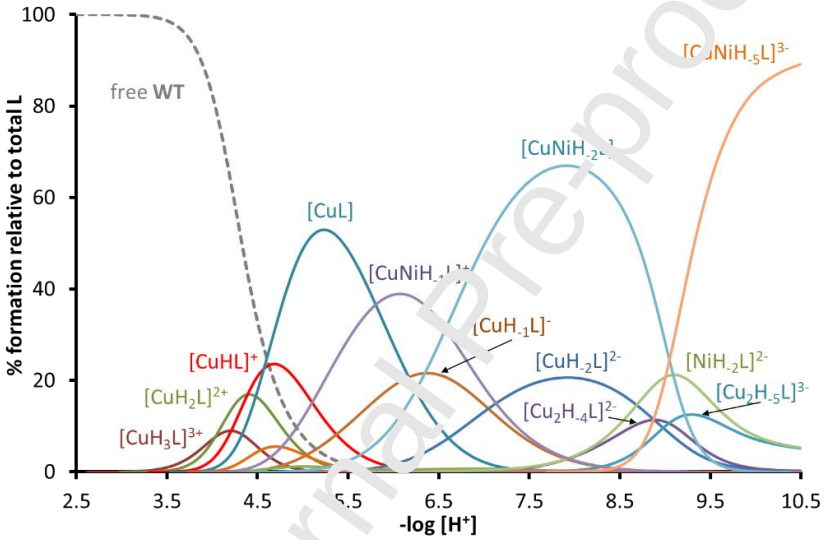

Fig. 6. Representative species distribution diagram for complex-formation in the ternary Cu(II)/Ni(II)/**WT** system, at T = 25 °C and I = 0.1 mol dm^{-3} (KCl). C_L = $C_{Cu(II)}$ = $C_{Ni(II)}$ = 1.0·10^{-3} mol dm^{-3}.

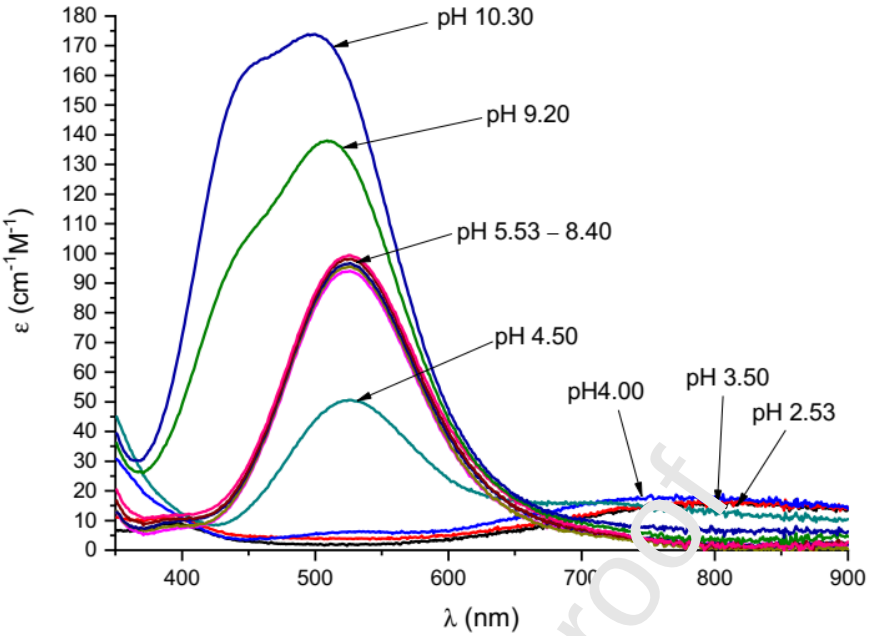

Fig. 7. Vis absorption spectra for Cu(II)/Ni(II) complexes with **WT**; C_L = 1.0·10^{-3} mol dm^{-3}, Cu(II):L = 0.8 : 1, Ni(II):L = 0.9 : 1.

Comparison of complex stability

When the various histidines of a peptide sequence have very similar chemical environments, spectroscopic techniques are unable to distinguish the behavior of each specific residue. Hence the need to study series of analogues, e.g. with the Ala-scan method used here. To obtain the required information, the stability of the complexes formed by the different mutants must be compared; however, this cannot be directly done through the stability constants, since the complexes have different stoichiometry and/or protonation degree. For this purpose, the parameters reported in Tables 10-12 have been calculated. The general meaning of these parameters is to give an overall estimation of the metal-ligand "affinity", under well-defined experimental conditions of pH and component concentration, which summarizes all the metal-ligand interactions that give rise to the speciation models described above. In particular, K_d (expressed as molarity, mol dm^{-3}) corresponds to the concentration of free metal when the ligand is half in the form of a complex (whatever its stoichiometry) and half not complexed [46]. K_d depends on pH but not on the ligand concentration and the smaller it is, the greater the complexes stability is. This parameter is widely used in biochemistry, assuming that, if the K_d value is equal to or less than the free metal concentration estimated (or measured) in the biological environment, then the ligand can "capture" the metal. A similar meaning can also be attributed to

pM (= -log[M]$_{free}$); in this case a higher value means that the ligand is more effective in metal sequestration [47]. The parameter $pL_{0.5}$, recently introduced by Sammartano and coworkers [48], refers to the quantity of ligand (expressed as -log[L]$_{tot}$) required to bind 50% of the metal present in traces (typically $[M]_{tot} = 1 \cdot 10^{-12}$ mol dm^{-3}). This parameter takes into account the action of all the other possible competing ligands present in solution (the speciation model of which must be known) and it is the greater the smaller the quantity of ligand required, i.e. the stronger the metal-ligand affinity. The values of K_d, pM and $pL_{0.5}$, at different pH and for all the systems studied are shown in Tables 10-12 together with reference values for the tetrapeptide DAHK-Am, corresponding to the ATCUN site of human albumin.

Table 10. Calculated dissociation constants (K_d/ mol dm^{-3}), pM and $pL_{0.5}$ values for Cu(II) complexes with the investigated peptides.

	K_d[(a)]		pCu[(b)]		$pL_{0.5}$[(c)]	
	pH = 7.4	**pH = 5.4**	**pH = 7.4**	**pH = 5.4**	**pH = 7.4**	**pH = 5.4**
WT	$2.35 \cdot 10^{-14}$	$9.95 \cdot 10^{-8}$	14.408	7.959	12.27	7.00
H3A	$4.03 \cdot 10^{-10}$	$1.65 \cdot 10^{-5}$	10.173	6.198	9.23	4.59
H4A	$4.48 \cdot 10^{-14}$	$2.26 \cdot 10^{-7}$	14.128	7.610	12.25	6.64
H8A	$4.63 \cdot 10^{-14}$	$1.31 \cdot 10^{-7}$	14.113	7.841	12.24	6.88
H4A/H8A	$4.26 \cdot 10^{-14}$	$2.52 \cdot 10^{-7}$	14.150	7.565	12.25	6.60
DAHK-Am[(d)]	$1.69 \cdot 10^{-14}$	$7.30 \cdot 10^{-8}$	14.550	8.093	12.28	7.14

[(a)] Kozlowski et al. [46]
[(b)] $[L]_{total} = 10^{-5}$ M and $[M]_{total} = 10^{-6}$ M; Crisponi et al. [47]
[(c)] Crea et al. [48]
[(d)] Speciation model taken from: Sokolowska et al. [40]

Table 11. Calculated dissociation constants (K_d/ mol dm^{-3}), pM and $pL_{0.5}$ values for Ni(II) complexes with the investigated peptides, at pH = 7.4.

	K_d	pNi	$pL_{0.5}$
WT	$6.19 \cdot 10^{-9}$	9.163	8.21
H3A	$5.24 \cdot 10^{-6}$	6.444	5.28
H4A	$5.89 \cdot 10^{-9}$	9.184	8.23
H8A	$1.13 \cdot 10^{-8}$	8.901	7.95
H4A/H8A	$4.72 \cdot 10^{-9}$	9.281	8.33
DAHK-Am[(d)]	$1.85 \cdot 10^{-9}$	9.689	8.73

[(d)] Speciation model taken from: Sokolowska et al. [40]

Table 12. Calculated dissociation constants (K_d/ mol dm^{-3}), pM and $pL_{0.5}$ values for Zn(II) complexes with the investigated peptides, at pH = 7.4.

	K_d	pZn	$pL_{0.5}$
WT	$3.17 \cdot 10^{-6}$	6.582	5.49
H3A	$4.44 \cdot 10^{-5}$	6.084	4.34
H4A	$6.99 \cdot 10^{-5}$	6.056	4.14
H8A	$1.70 \cdot 10^{-4}$	6.024	3.76
H4A/H8A	$2.65 \cdot 10^{-4}$	6.016	3.56

As for the Cu(II) complexes, from Table 10 it is clear that the best ligand in the series is human albumin at both pH 7.4 and 5.4: although the coordination site is always of the ATCUN type and therefore the binding mode is very similar for all peptides (with the exception of **H3A**), the particular albumin sequence is favored probably due to the presence of the aspartic acid residue, whose side carboxyl group can participate in the metal complexation through an axial interaction [49, 50]. In the series of Hpn protein analogues, **WT** forms the most stable complexes: the presence of an extra histidine residue and the possibility of forming different complexes with identical stoichiometry but different set of donor atoms is probably the reason of this greater affinity. The differences between the **H4A**, **H8A** and **H4A/H8A** ligands, which have an identical ATCUN site but different combinations of additional histidines, are of minor importance, although it can be observed that the **H4A/H8A** peptide, which only possesses one histidine in position 3 (and which consequently cannot form binuclear complexes), has the lowest affinity. A significantly lower strength as Cu(II) ligand is shown by **H3A**, where the histidine in position 3, responsible for the ATCUN sequence, was replaced by alanine. As expected, the His-3 residue is crucial to confer high Cu(II) binding affinity to the studied peptides like in human albumin. Similar considerations can be deduced from the competition diagram reported as Supplementary Material (Fig. S53, SI†), which allow to compare the strength of the ligands in a wide pH range.

Also in the case of Ni(II) complexes, the best ligand proved to be DAHK-Am (Table 11). Surprisingly, the peptide of the series which has the second-best affinity for Ni(II) is **H4A/H8A**, which contains less histidines than all the others. Evidently, the ATCUN binding motif, which leads to the formation of strictly square-planar Ni(II) complexes plays a major role and the presence of additional histidines is negligible, or even disturbing, when moving towards neutral and alkaline pH, as it can be observed from the competition diagram of Fig. S54, SI†. On the other hand, His-8

(which is absent in **H8A**) seems to contribute to the stability of the system; moreover, as discussed in the previous section, the obtained CD data for **WT** and **H4A** undergo a shape variation at pH > 9, suggesting that His-8 is somehow involved in coordination at alkaline pH. Once again, the lack of the His residue in position 3 strongly penalizes the **H3A** peptide, as already observed in the case of Cu(II).

The coordination modes of the Zn(II) ion are very different from those of Cu(II) and Ni(II), as described above. In this case, the number of histidine residues of the peptide plays a major role in establishing its affinity towards the metal. The results reported in Table 12 and Fig. S55 SI† show that **WT** is by far the strongest ligand of the series, at acidic pH; it is the only one which can form Zn(II) complexes with three imidazole nitrogens as donor atoms. In contrast, **H4A/H8A** is the weakest ligand; in fact, it possesses only one histidine. Moreover, the zinc affinity is significantly lower for the **H3A** and **H8A** peptides than for the **H4A** ligand, although all the three of them possess two histidines. This result suggests a minor role for His-4, with respect to His-3 and His-8, in zinc chelation.

Finally, the data of Tables 10-12 clearly show that, under the same experimental conditions, the N-terminal domain of Hpn (represented by **WT**) has great selectivity towards the metals studied with affinities in the following order: Cu(II) >> Ni(II) > Zn(II). Similar considerations also apply to the other peptides. As already described above, a recent study [13] reported, in the case of Ni(II), a K_d value for the Hpn protein of $7.89 \cdot 10^{-8}$. It can be considered in a reasonably good agreement with the value measured in the present work for the Ni(II)/**WT** system ($6.19 \cdot 10^{-9}$ M, Table 11), also taking into account that the experimental conditions are rather different. Hence, it can be deduced that the amino-terminal ATCUN site of Hpn plays an important role in the nickel coordination. On the contrary, in the case of Zn(II), the K_d value measured here for the peptide **WT** ($3.17 \cdot 10^{-6}$ mol dm^{-3}, Table 12) is much higher than that reported by Wegner et al. for the Hpn protein ($1.03 \cdot 10^{-9}$ mol dm^{-3}). This is attributable to the fact that Hpn has other binding sites rich in histidine and cysteine residues which have a greater affinity for zinc than the amino-terminal domain.

Conclusions

The studied peptides proved to be good chelators for divalent copper, nickel and zinc ions. With the exception of **H3A**, all the investigated sequences contain a very efficient Cu(II) and Ni(II)

ATCUN-binding site (N_{Im}, NH_2, $2N^-$) which is confirmed to confer great stability to copper and nickel complexes. Furthermore, the presence of additional histidines in position 4 and 8 allows the formation of stable homo- and hetero- binuclear complexes. In the case of Zn(II) ion, the ligand effectiveness is not strictly affected by the presence of the ATCUN sequence, but most likely depends on the number of available histidines, which act as multiple metal anchoring sites and allow the formation of macrochelate systems. The binding strength of the N-terminus of Hpn protein has been compared with that of the other studied binding sites of Hpn, i.e the two motifs containing a double cysteine residue in the positions 38–42 and 51–55 [17] and the poly-histidine sequence in the positions 18–26 [14]. The corresponding competition diagrams are reported as Supplementary Information (Figs. S56, S57 SI†). The -Cys-Cys- motifs are stronger than the N-terminal ATCUN site, both for Ni(II) and Zn(II) coordination. On the other hand, the poly-His sequence corresponding to the 18-26 domain of Hpn can compete with the N-terminus only at acidic pH value. In view of the fact that Hpn can bind up to five Ni(II) ions, we can suggest that all these four studied binding sites are involved in nickel trafficking. It looks reasonable that, at low nickel levels, the cysteine binding sites are saturated with nickel before than His binding sites.

The formation of binuclear Cu(II) complexes have been extensively studied; from the obtained results one can generally assume that the first Cu(II) ion interacts with the peptide at the very effective N-terminal ATCUN site (if present), while a second Cu(II) ion can further coordinate the histidine residues in position 4 and 8. However, His-8 seems to be the favorite site, due to the possibility to further coordinate the amide nitrogen towards the N-terminal direction, forming a stable 5/6-membered chelate rings.

As expected from the Irving-Williams series [51], the N-terminal domain of Hpn displays metal-binding affinities in the order Zn(II) < Ni(II) << Cu(II). In particular, this means that Cu(II), even if present in low amount, can replace Ni(II) in the Hpn protein coordination. Moreover, the **WT** model peptide was proved to form hetero-binuclear complexes, where the ATCUN sequence interacts exclusively with Cu(II) while nickel preferentially binds the histidine residue in position 8 (second binding site) to form its typical square planar complex (N_{Im}, $3N^-$)(see Fig. 8). In the interaction of Cu(II) with a binary Ni(II)/**WT** complex, the nickel ion can be either released or even moved from the ATCUN site to the second binding site. In both cases the activity of Hpn protein is disturbed. In fact, Figs. S58, S59 SI† show that, in the presence of only a 20% of Cu(II) with respect to Ni(II), not only mixed Cu(II)/Ni(II) species are formed in the entire pH range, but, at neutral pH, some Ni(II) is still not complexed (see Fig. S23 SI† for the sake of comparison in the absence of

copper). When thinking about possible antimicrobial strategies, a suitable Cu(II) complex, sufficiently stable to reach the bacterium but weaker that that formed with Hpn, could be employed as a pharmacophore, with the aim of producing a "ligand exchange" reaction, where Cu(II) ions substitute Ni(II) ions at the Hpn ATCUN domain; in a possible additional second step, the released Ni(II) ions could even be sequestered by the metal-free pharmacophore and eliminated. This action would partially inhibit the Hpn efficiency in Ni(II) recruitment and storage, thus helping the nutritional immunity mechanism to starve the pathogen. A similar action could also be obtained with the more safe Zn(II) ion, but it would require very high Zn(II) concentration, since its affinity for Hpn, at least as far as the N-terminus is concerned, is much lower than that of Ni(II). Anyway, Fig. S60 SI† shows that, in the presence of a 10-fold excess of Zn(II) with respect to Ni(II), the most acidic pH values are dominated by Zn(II) complexes, and, at neutral pH, about 30% of the peptide is engaged in zinc binding.

The strategy of distressing bacterial nickel homeostasis by means of competing metals (or ligands) looks promising in order to find new therapeutic ways to eradicate *H. pylori* and a detailed understanding of metal binding modes in bacterial metal chaperones is a valuable "brick in the wall" which aims to stop the pathogens from spreading.

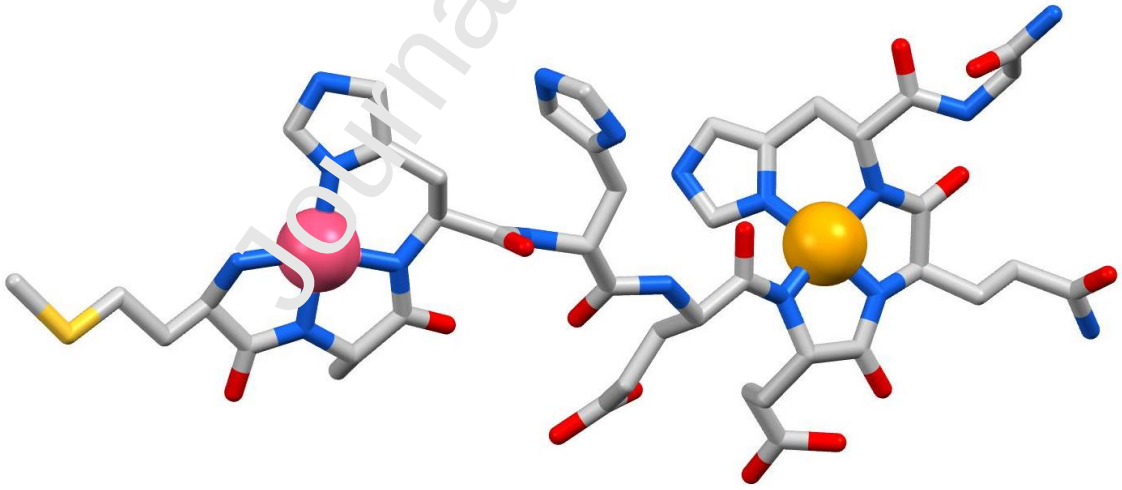

Fig. 8. Proposed molecular structure for the hetero-binuclear complex $[CuNiH_{-5}L]^{3-}$. Cu(II) atom (in purple) is bound to the ATCUN site (N_{Im}, NH_2, $2N^-$), Ni(II) atom (in yellow) displays a (N_{Im}, $3N^-$) coordination mode.

Acknowledgements

Financial support by University of Ferrara (FAR 2020), the National Science Centre (UMO-2017/26/A/ST5/00364 and 2017/26/A/ST5/00363) and by the Erasmus+ Programme are gratefully acknowledged. This paper is based upon work from COST Action CA18202, NECTAR – Network for Equilibria and Chemical Thermodynamics Advanced Research, supported by COST (European Cooperation in Science and Technology). The authors would thank dr. Claudia Stevanin for her assistance in the acquisition and interpretation of some ESI-MS spectra.

References

[1] C. de Martel, J. Ferlay, S. Franceschi, J. Vignat, F. Bray, D. Forman, M. Plummer, The Lancet Oncology, 13 (2012) 607-615.
[2] Z. Saylor, R. Maier, Microbiology, 164 (2018) 1059-1068.
[3] D.R. Scott, D. Weeks, C. Hong, S. Postius, K. Melchers, G. Sachs, Gastroenterology, 114 (1998) 58-70.
[4] N.-C. Ha, S.-T. Oh, J.Y. Sung, K.A. Cha, M.H. Lee, B.-H. Oh, Nat. Struct. Biol., 8 (2001) 505-509.
[5] J.W. Olson, R.J. Maier, Science, 298 (2002) 1788.
[6] J.V. Gilbert, J. Ramakrishna, F.W. Sunderman, A. Wright, A.G. Plaut, Infect. Immun., 63 (1995) 2682.
[7] R.J. Maier, S.L. Benoit, S. Seshadri, Biometals, 20 (2007) 655-664.
[8] S. Seshadri, S.L. Benoit, R.J. Maier, J. Bacteriol., 189 (2007) 4120-4126.
[9] G. Wang, P. Alamuri, R.J. Maier, Mol. Microbiol., 61 (2006) 847-860.
[10] H. Zeng, G. Guo, X.H. Mao, W. De Tong, Q.M. Zou, Curr. Microbiol., 57 (2008) 281-286.
[11] R. Ge, Rory M. Watt, X. Sun, Julian A. Tanner, Q.-Y. He, J.-D. Huang, H. Sun, Biochem. J., 393 (2005) 285-293.
[12] R.M. Shelake, Y. Ito, J. Masumoto, F.H. Morita, H. Hayashi, PLoS ONE, 12 (2017) e0172182-e0172182.
[13] S.V. Wegner, E. Ertem, M. Sunbul, C. He, Chem. Sci., 2 (2011) 451-456.
[14] D. Witkowska, R. Politano, M. Rowinska-Zyrek, R. Guerrini, M. Remelli, H. Kozlowski, Chem. – Eur. J., 18 (2012) 11088-11099.
[15] M. Rowinska-Zyrek, J. Zalewska-Czerwinska, A. Zawilak-Pawlik, H. Kozlowski, Dalton Trans., 43 (2014) 8976-8989.
[16] M. Rowinska-Zyrek, D. Witkowska, S. Potocki, M. Remelli, H. Kozlowski, New J. Chem., 37 (2013) 58-70.
[17] M. Rowinska-Zyrek, D. Witkowska, S. Bielinska, W. Kamysz, H. Kozlowski, Dalton Trans., 40 (2011) 5604-5610.
[18] D. Witkowska, S. Bielinska, W. Kamysz, H. Kozlowski, J. Inorg. Biochem., 105 (2011) 208-214.
[19] N.M. Chiera, M. Rowinska-Zyrek, R. Wieczorek, R. Guerrini, D. Witkowska, M. Remelli, H. Kozlowski, Metallomics, 5 (2013) 214-221.
[20] C. Harford, B. Sarkar, Acc. Chem. Res., 30 (1997) 123-130.
[21] N.L. Benoiton, Chemistry of Peptide Synthesis, Taylor & Francis, London, 2005.
[22] N.A. Sole, G. Barany, J. Org. Chem., 57 (1992) 5399-5403.
[23] P. Gans, A. Sabatini, A. Vacca, Dalton Trans., (1985) 1195-1200.
[24] P. Gans, B. O'Sullivan, Talanta, 51 (2000) 33-37.
[25] G. Gran, Acta Chem. Scand., 4 (1950) 559-577.
[26] P. Gans, A. Sabatini, A. Vacca, Talanta, 43 (1996) 1739-1753.
[27] G. Arena, R. Cali, E. Rizzarelli, S. Sammartano, Therm. Acta, 16 (1976) 315-321.
[28] C.F. Baes, M.R. S., The Hydrolysis of Cations John Wiley & Sons, Ltd, New York, 1976.
[29] L. Alderighi, P. Gans, A. Ienco, D. Peters, A. Sabatini, A. Vacca, Coord. Chem. Rev., 184 (1999) 311-318.

[30] L.D. Pettit, H.K.J. Powell, The IUPAC Stability Constants Database, Royal Society of Chemistry, London, 1992-2000.
[31] I. Sóvágó, K. Várnagy, N. Lihi, Á. Grenács, Coord. Chem. Rev., 327-328 (2016) 43-54.
[32] H. Sigel, R.B. Martin, Chem. Rev., 82 (1982) 385-426.
[33] J. Peisach, W.E. Blumberg, Arch. Biochem. Biophys., 165 (1974) 691-708.
[34] P.G. Daniele, E. Prenesti, G. Ostacoli, Dalton Trans., (1996) 3269-3275.
[35] D. Bellotti, C. Tocchio, R. Guerrini, M. Rowińska-Żyrek, M. Remelli, Metallomics, 11 (2019) 1988-1998.
[36] K. Krupa, M. Korabik, T. Kowalik-Jankowska, J. Inorg. Biochem., 201 (2019) 110819.
[37] C. Conato, H. Kozłowski, P. Młynarz, F. Pulidori, M. Remelli, Polyhedron, 21 (2002) 1469-1474.
[38] M. Rowińska-Żyrek, H. Kozłowski, Nickel Binding Sites – Coordination Modes and Thermodynamics, in: The Biological Chemistry of Nickel, The Royal Society of Chemistry, 2017, pp. 43-59.
[39] W. Bal, M. Jeżowska-Bojczuk, K.S. Kasprzak, Chem. Res. Toxicol., 10 (1997) 906-914.
[40] M. Sokolowska, A. Krezel, M. Dyba, Z. Szewczuk, W. Bal, Eur. J. Biochem., 269 (2002) 1323-1331.
[41] M. Peana, K. Zdyb, S. Medici, A. Pelucelli, G. Simula, E. Gumienna-Kontecka, M.A. Zoroddu, J. Trace Elem. Med Biol., 44 (2017) 151-160.
[42] J.D. Van Horn, G. Bulaj, D.P. Goldenberg, C.J. Burrows, J. Biol. Inorg. Chem., 8 (2003) 601-610.
[43] W. Bal, J. Lukszo, K.S. Kasprzak, Chem. Res. Toxicol., 9 (1996) 535-540.
[44] W. Bal, H. Kozlowski, R. Robbins, L.D. Pettit, Inorg. Chim. Acta, 231 (1995) 7-12.
[45] Á. Grenács, A. Kaluha, C. Kállay, V. Jószai, D. Sanna, I. Sóvágó, J. Inorg. Biochem., 128 (2013) 17-25.
[46] H. Kozlowski, M. Łuczkowski, M. Remelli, Dalton Trans., 39 (2010) 6371-6385.
[47] G. Crisponi, M. Remelli, Coord. Chem. Rev., 252 (2008) 1225-1240.
[48] F. Crea, C. De Stefano, C. Foti, D. Milea, S. Sammartano, Curr. Med. Chem., 21 (2014) 3819-3836.
[49] J.P. Laussac, B. Sarkar, J. Biol. Chem., 255 (1980) 7563-7568.
[50] J.P. Laussac, B. Sarker, Biochemistry, 23 (1984) 2832-2838.
[51] H. Irving, R.J.P. Williams, J. Chem. Soc., (1953) 3192-3210.